

# Reservoir quality evaluation and prediction in ultra-deep tight sandstones in the Kuqa depression, China

Jin Lai<sup>a,b,\*</sup>, Dong Li<sup>b</sup>, Tianyu Bai<sup>b</sup>, Fei Zhao<sup>b</sup>, Yong Ai<sup>c</sup>, Hongkun Liu<sup>d</sup>, Deyang Cai<sup>c</sup>, Guiwen Wang<sup>a,b,\*\*</sup>, Kangjun Chen<sup>e</sup>, Yuqiang Xie<sup>b</sup>

<sup>a</sup> State Key Laboratory of Petroleum Resources and Prospecting, China University of Petroleum, Beijing, 102249, China

<sup>b</sup> College of Geosciences, China University of Petroleum, Beijing, 102249, China

<sup>c</sup> Research Institute of Petroleum Exploration and Development, Tarim Oilfield Company, CNPC, Korla, 841000, Xinjiang, China

<sup>d</sup> China France Bohai Geoservices Company Limited, Zhanjiang, 524000, Guangdong, China

<sup>e</sup> Development Division, PetroChina Southwest Oil & Gas Field Company, Chengdu, 610051, Sichuan, China

## ARTICLE INFO

### Keywords:

Ultra-deep sandstone  
Fracture  
Diagenetic facies  
Depositional facies  
Tight sandstone  
Kuqa depression

## ABSTRACT

Core, thin sections, cathodoluminescence (CL), scanning electron microscopy (SEM), conventional well logs and image logs are used to unravel depositional microfacies, diagenetic facies and fractures in the deeply buried (6000–8100 m) Cretaceous Bashijiqike ( $K_1bs$ ) and Baxigai ( $K_1bx$ ) Formations in Kuqa depression of the Tarim Basin. Results show that depositional microfacies in core and well log data include distributary channel, river mouth bar and distributary bay deposits of fan-braided delta fronts as well as lacustrine deposits. We establish well log predictable models of depositional microfacies using conventional and image logs. The Cretaceous sandstones experienced low to medium mechanical compaction and low intensity dissolution. Dominant diagenetic minerals are carbonate cements, clay minerals and minor amounts of quartz cements. The pore spaces are primarily intergranular pores and rare dissolution pores. We identify three diagenetic facies according to compaction state and diagenetic minerals, including carbonate cemented facies, tightly compacted facies, and facies having limited compaction and lacking cement (slightly cemented and compacted facies). We use well log characteristics to interpret diagenetic facies in areas without core data. Fractures are also elements of reservoir quality, including vertical opening-mode fractures, high to medium dip angle fractures, low angle fractures that probably include small faults and horizontal fractures. Fractures include open, partially open, and closed (sealed) fractures. We used image logs to identify fracture attributes, and calculate fracture density, porosity, aperture, and length. Depositional microfacies and diagenetic facies determine the primary intergranular pores and diagenesis subsequently modified secondary pore spaces. Natural fractures acted as both reservoir porosity (probably less than 1%) and as hydrocarbon flow channels accounting for elevated permeability. We evaluate and predict reservoir quality by superposing depositional microfacies, diagenetic facies and fracture occurrence.

## 1. Introduction

In tight sandstones (porosity <10%, in situ permeability <0.1 mD) (Holditch, 2006), especially, ultra-deeply buried (>6000 m) tight sandstones, lack of sandstone porosity represents a great hydrocarbon exploration risk (e.g., Dutton et al., 1993; Lai et al., 2017a). Consequently, prediction of sandstone porosity has been the focus of extensive research (e.g., Lander and Walderhaug, 1999; Mansurbeg et al., 2008; Ajdukiewicz and Lander, 2010; Morad et al., 2010). Sandstone porosity

(and permeability) evaluation is commonly called ‘reservoir quality assessment’. But owing to disciplinary divides (e.g., Laubach et al., 2010), fractures are not typically considered as part of reservoir quality assessment, despite observations that fractures in tight sandstone are widespread and commonly contribute to reservoir permeability (e.g., Laubach, 2003; Solano et al., 2011; Lai et al., 2018). Although individually, reservoir quality evaluation and prediction in sandstones includes work on depositional microfacies (Bjørlykke, 2014; El Sawy et al., 2020), diagenesis (Lai et al., 2016; Zhang et al., 2022) and fracture

\* Corresponding author. China University of Petroleum (Beijing), 18 Fuxue Road, Changping, Beijing, 102249, China.

\*\* Corresponding author. State Key Laboratory of Petroleum Resources and Prospecting, China University of Petroleum, Beijing, 102249, China.

E-mail addresses: [sisylaijin@163.com](mailto:sisylaijin@163.com) (J. Lai), [wanggw@cup.edu.cn](mailto:wanggw@cup.edu.cn) (G. Wang).

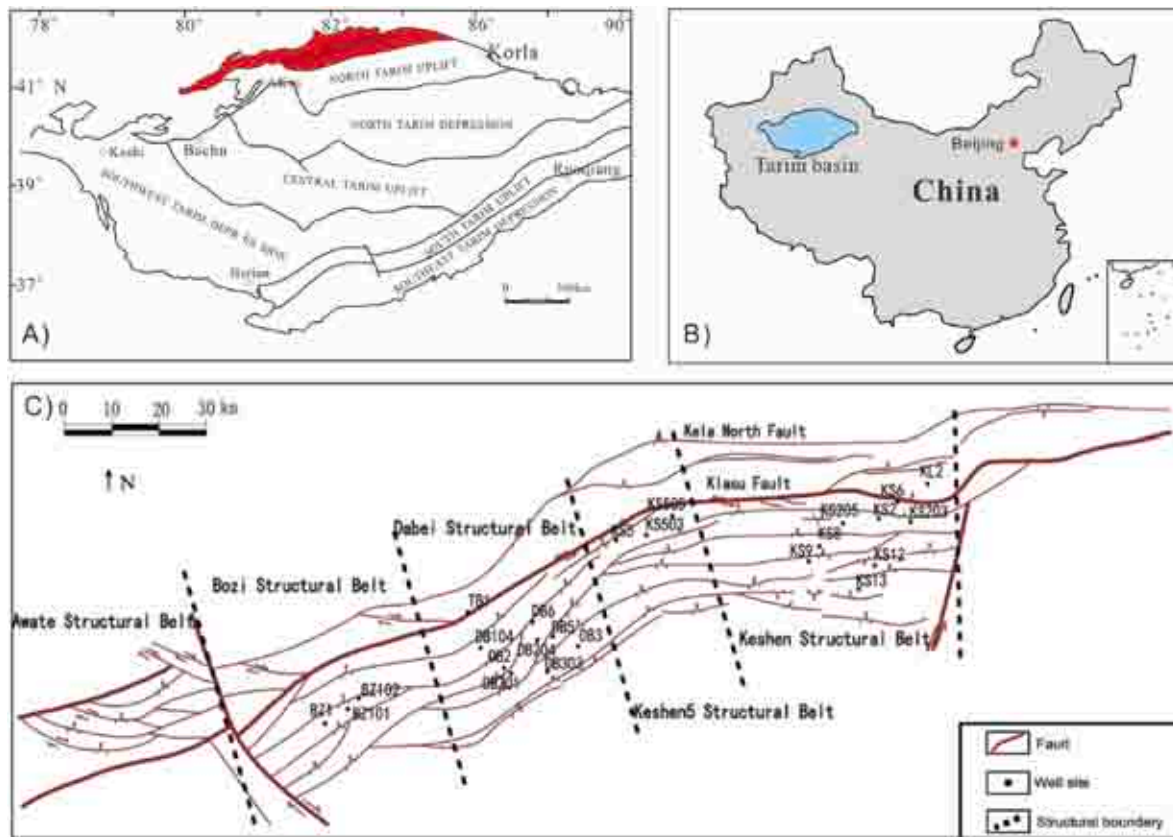


Fig. 1. Maps show the structural division of the Kuqa Depression within North Tarim basin of West China (Jin et al., 2008; Shen et al., 2017; Lyu et al., 2017; Wu et al., 2020).

(Busch et al., 2021; Lai et al., 2022a; Lyu et al., 2022), for deep and ultra-deep tight sandstones little systematic work has comprehensively integrated depositional microfacies, diagenetic facies, and fracture. Here we explore the porosity and permeability of deeply buried (ca. 8000 m) sandstones by evaluating both sandstone (host rock) diagenesis and fracture occurrence.

Deeply buried sandstones commonly show low porosity, complex pore assemblages, and strong attribute heterogeneity (e.g., Dutton et al., 1993; Zou et al., 2012; Lai et al., 2018). Reservoir quality is a comprehensive reflection of initial depositional microfacies, and subsequent diagenetic alterations (diagenetic facies) (e.g., Ramm, 2000; Rossi et al., 2001; Salem et al., 2005; Ozkan et al., 2011; Zhang et al., 2015; Higgs et al., 2017) as well as the formation and attributes of fractures (e.g., Lorenz, 1999; Laubach, 2003; Almansour et al., 2020), which themselves typically participate in diagenesis (e.g. Laubach et al., 2019).

The Lower Cretaceous Bashijiqike ( $K_1bs$ ) and Baxigai ( $K_1bx$ ) Formations in the Kuqa depression, which are buried as deep as 8000m and have average porosity <10% and intrinsic permeability <0.1 mD, are typical ultra-deeply buried tight sandstones (Lai et al., 2017a; Xin et al., 2022). Though ultra-deeply buried and with porosity of less than 10% the sandstones are gas bearing and many high gas productivity wells have revealed the prospect for effective natural gas exploration (Lai et al., 2017a). Reservoir quality of sandstones at shallow depth is mainly controlled by depositional microfacies, however, the ultra-deeply buried sandstones are controlled by the coupling of depositional microfacies, diagenetic facies and fractures. Consequently, the superposition of depositional microfacies, diagenetic facies and fractures is used for reservoir quality evaluation and prediction in the ultra-deep buried sandstones (Nabawy, 2018; Radwan et al., 2021).

Here we show that the depositional microfacies and diagenetic facies control the matrix porosity, while fractures enhance hydrocarbon

productivity. The depositional microfacies, diagenetic facies and fractures are superimposed together for reservoir quality evaluation and prediction for the Cretaceous ultra-deeply buried tight sandstones in Kuqa depression. Firstly we recognize the depositional microfacies using core observation and well logs. Secondly we classified the diagenetic facies through thin section and SEM, and then build a predictive model for diagenetic facies using well logs. Thirdly we characterize the fractures using core and image log observation. We predict productive zones ('sweet spots') by superposing depositional microfacies, diagenetic facies and fracture, and find sweet spots coincide with elevated oil well production response test data. The integration of depositional microfacies, diagenetic facies and fracture can be used for reservoir quality evaluation and prediction in ultra-deep tight sandstones.

## 2. Geological setting

The Kuqa depression is a Mesozoic to Cenozoic foreland depression located in the northern Tarim Basin (Shi et al., 2004; Zhang and Huang, 2005; Zeng et al., 2010; Nian et al., 2016; Teng et al., 2020). The Kuqa depression is the transition zone between the Tianshan Mountains and the Tarim Basin (Feng et al., 2018), and has experienced a long and complex evolutionary history (Ju and Wang, 2018). Two sags namely the Baicheng and Yangxia Sags, and three structural belts including a northern monocline, Kelasu and Qiluitang structural belt are recognized (Ju and Wang, 2018) (Fig. 1). The complex tectonic evolution resulted large numbers of thrust faults and related folds. In this setting, the formation of fractures is to be expected and many are known from the subsurface (Ju and Wang, 2018; Feng et al., 2018; Zheng et al., 2020). The formation of fractures is therefore a potential control on flow behavior (reservoir quality) (Zeng et al., 2010).

Mesozoic-Cenozoic strata are thick, up to 11000 m (Zou et al., 2006).

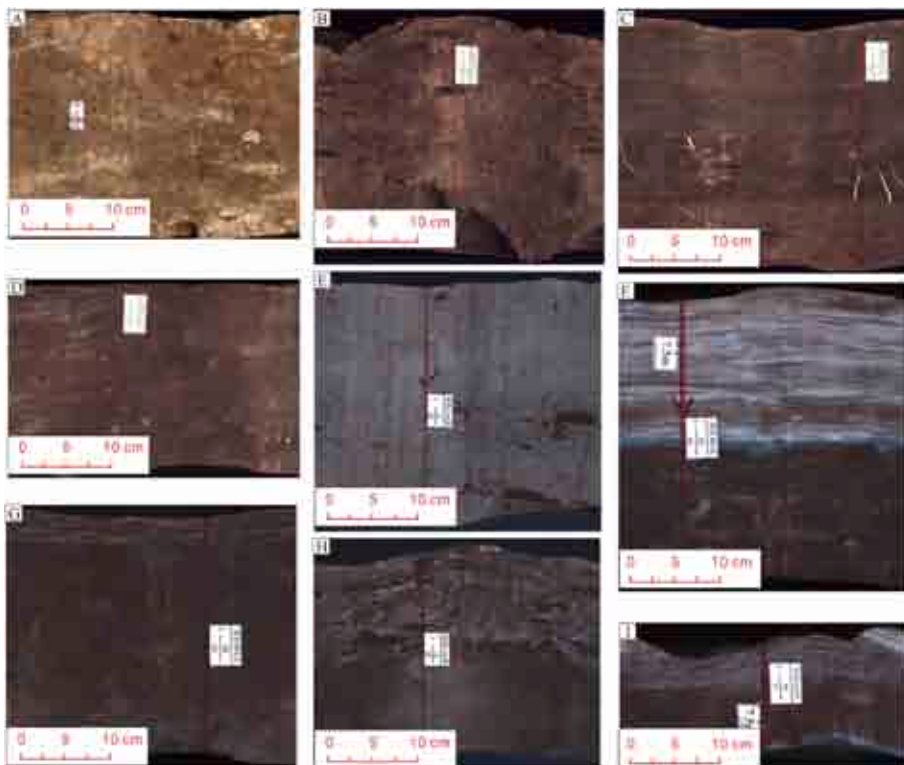


**Fig. 2.** Core photos (unfolded drawings) showing the lithology and sedimentary structures in Bashijiqike Formation in Kuqa depression.

- A. Conglomerates, Well B1, 4373.68 m
- B. Pebbly sandstones, Well B101, 6918.4 m
- C. Fine-grained sandstones with inclined bedding, Well B101, 6916.1m
- D. Fine-grained sandstones with trough cross beddings, Well B101, 6916.2 m
- E. Massive medium grained sandstones, Well B104, 6843.2
- F. Wavy bedding in the siltstones, Well B103, 7220 m
- G. Massive mudstones, Well B103, 7219.28 m
- H. Reactivation surfaces, Well B104, 6844.8m
- I. Scour surfaces, Well B103, 7316.6m.

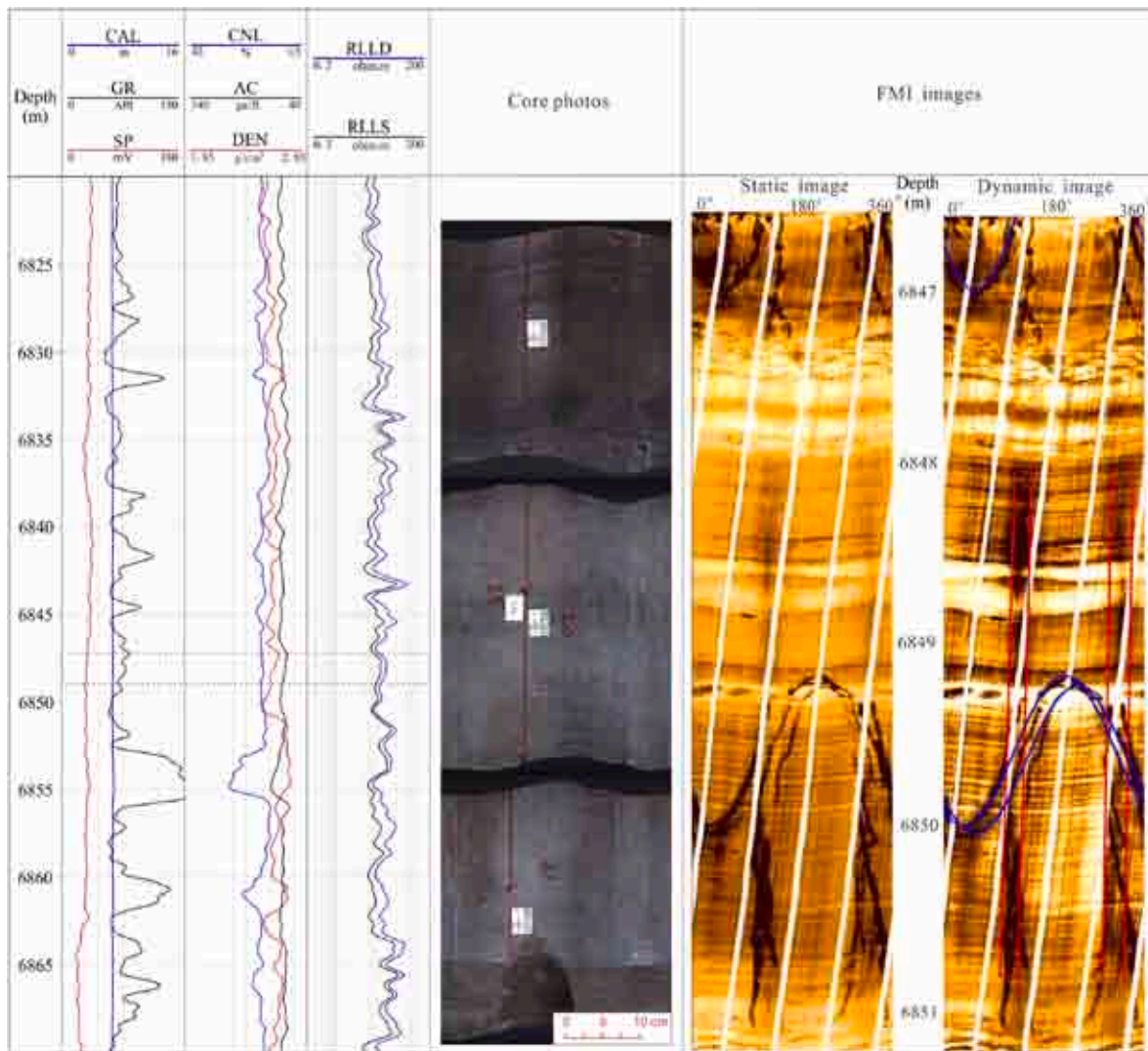


**Fig. 3.** Conventional well and image log responses of distributary channel in Bozi-Dabei Wellblock of Kuqa depression. The distributary channel facies is recognized as low GR, and image logs are recognized as bright characteristics with cross beddings.

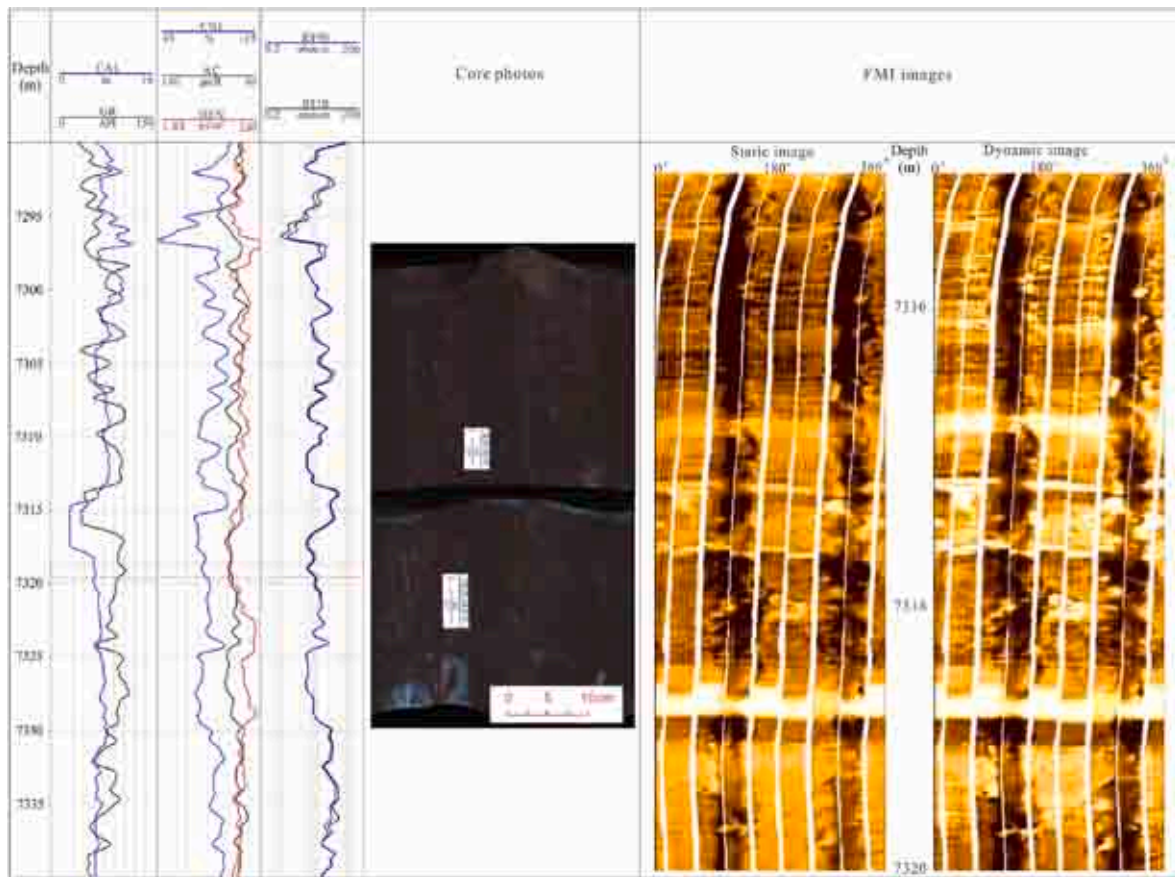
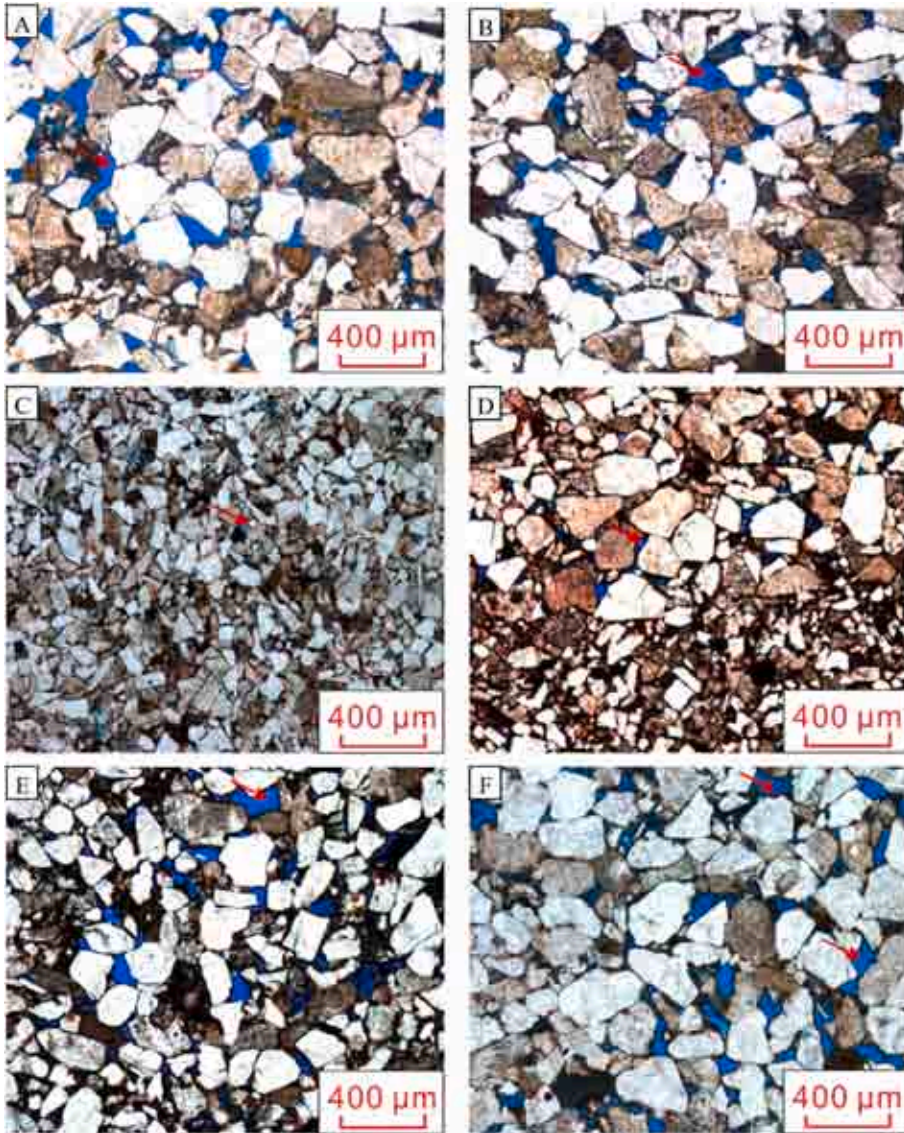
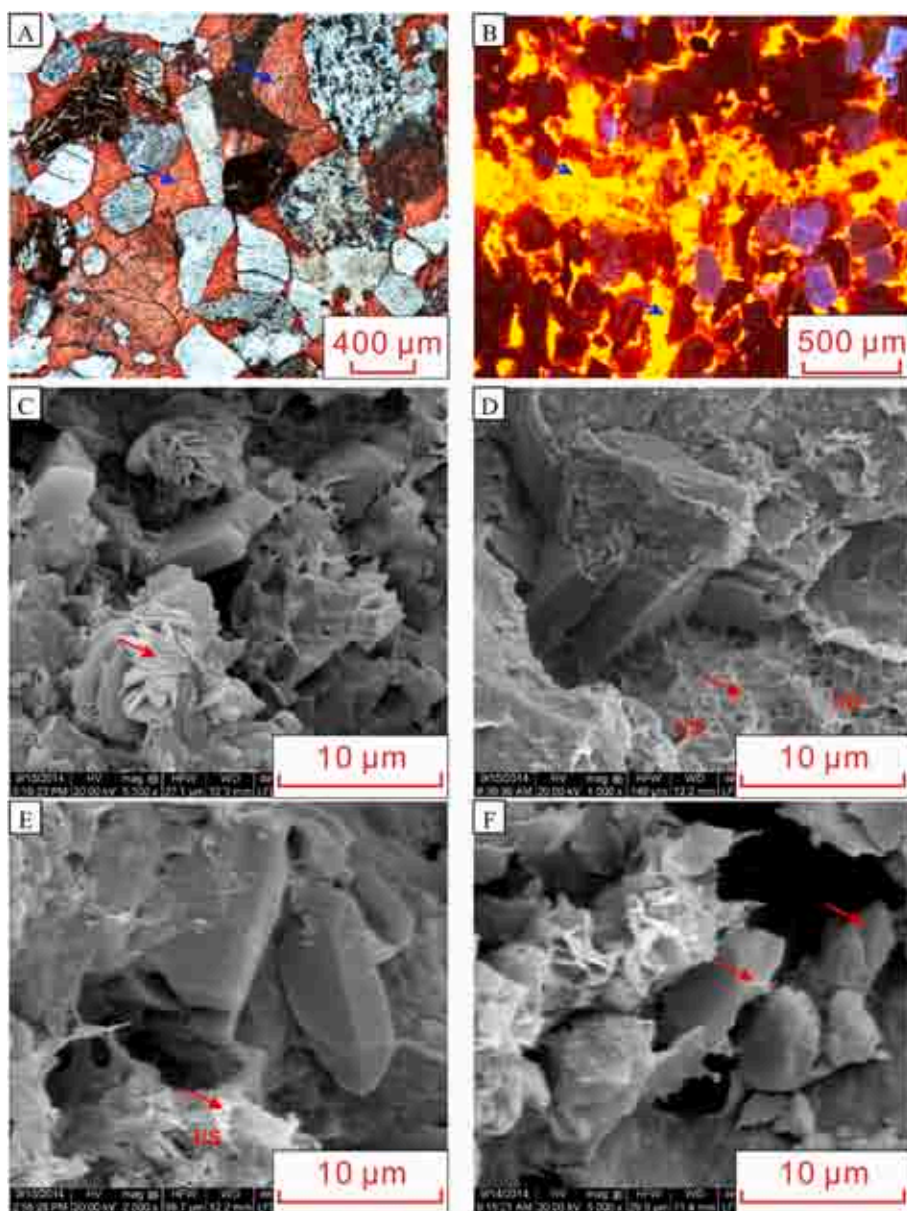


Fig. 4. Conventional well and image log responses of distributary bay in Bozi-Dabei wellblock of Kuqa depression (The distributary bay facies is recognized as high GR, and image logs are recognized as dark massive characteristics.)



**Fig. 5.** Thin section images showing the compaction and dissolution degree of Bashijiqike formation in Bozi-Dabei wellblock of Kuqa depression

- A. Abundance of intergranular pores (arrow), low to moderate degree of compaction (note there are grain-coating clays), Well B8, 8083.12 m
- B. Low to moderate degree of compaction (note there are grain-coating clays), abundant in intergranular pores (arrow), Well B8, 8081.84 m
- C. Extensive compaction and minor pores (arrow), Well B301, 5854.45m
- D. High degree of compaction and minor pores (arrow), Well B9, 7685.49 m
- E. Abundance in intergranular pores (note there are grain-coating clays), while dissolution pore (arrow) is rare, Well B9, 7689.32 m
- F. Minor amounts of dissolution pores, abundant in intergranular pores and minor pores (arrow), Well B9, 7689.91m.



**Fig. 6.** Photomicrographs showing diagenetic minerals of the Bashijiqike sandstones in Bozi-Dabei wellblock of Kuqa depression.

A. Calcite cements (arrow), Well B301, 5884.25 m  
 B. Carbonate cements with bright orange–red and yellow luminescence patterns (arrow), Well B101, 6918.62m, CL images  
 C. Gypsum filling in the pore spaces (arrow), Well B101, 6917.81m  
 D. Mixed layered illite/smectite (arrow), Well B102, 6769.74 m  
 E. Mixed layered illite/smectite (arrow), Well B101, 6917.42 m  
 F. Minor amount of quartz cements (arrow), Well B102, 6758.04m. (For interpretation of the references to color in this figure legend, the reader is referred to the Web version of this article.)

The Triassic–Jurassic coal bearing formations (Jurassic Yangxia formation ( $J_{1y}$ ), Triassic Karamay ( $T_{2k}$ ) and Huangshanjie ( $T_{3h}$ ) formations) act as the source rocks (Shen et al., 2017; Xin et al., 2022). The Kumugeliemu group ( $E_{1-2km}$ ) thick-layer gypsum salt rock acts as the regional cap rocks in the Kuqa depression. The Bashijiqike Formation was deposited in a fan-braided deltaic depositional setting, and can be divided into three members ( $K_{1bs_3}$ ,  $K_{1bs_2}$ ,  $K_{1bs_1}$ ). In addition, the Baxigai Formation is divided into two members ( $K_{1bx_1}$ ,  $K_{1bx_2}$ ) (Xin et al., 2022). The lithologies of Bashijiqike and Baxigai Formation are dominated by red to brown, sandstones (mainly fine to medium-grained), conglomerates, and pebbly sandstone as well as mudstone (Wang et al., 2013; Sun et al., 2017). The  $K_{1bs_3}$  member (third member of Bashijiqike Formation) was formed in a fan delta front environment, while the  $K_{1bs_2}$  and  $K_{1bs_1}$  members were deposited in a braided delta front environment (Wang et al., 2013). Typical depositional microfacies recognized by core and well log interpretation in the Bashijiqike Formation include distributary channel, river mouth bar and distributary bay as well as lacustrine microfacies (Xu et al., 2004; Lai et al., 2017a).

The South Tianshan was the source of Cretaceous sediments in the Kuqa depression. Depositional environment of Bashijiqike and Baxigai

Formation is recognized as fan to braided delta in arid to semiarid paleoclimate (Wang et al., 2013; Lai et al., 2017a). The Cretaceous strata had experienced extensive tectonic evolution, and many folds and faults are present in the Kuqa depression. Additionally, the sandstones are heavily fractured and exist in an active tectonic setting (Nian et al., 2017, 2021).




### 3. Samples and methods

Cores were taken from 10 recently drilled vertical wells. About 100 m of 10-cm-diameter core was obtained. Core surfaces were scanned for 360° with the aim to record lithology, sedimentary structures as well as to document the presence of fractures. The core plug samples span a wide depth range from 6000 to 8100 m.

Helium porosity and permeability tests were performed on 100 samples. Thin sections impregnated with blue epifluorescent epoxy were used to detect porosity and micro-fractures as well as composition and texture (framework grains, grain size, sorting), pore spaces (intergranular and intragranular), and diagenetic minerals and textures.

An optical cathodoluminescence microscope was used to

**Table 1**  
Diagenesis and diagenetic minerals as well as pore spaces for various diagenetic facies.

Diagenetic facies	Composition, texture and pore spaces	Diagenesis and diagenetic minerals	Pore spaces	Thin section images
Tightly compacted facies	Rich in detrital clays; Very fine-grained, poorly sorted	Highest degree of mechanical compaction, rare in intergranular porosity	No evident pores	 B9, 7686.33m
Carbonate cemented facies	Abundant in carbonate cements; Fined to medium grained	Highest amount of carbonate cements (>10%), mechanical compaction is limited	No evident pores	 B301, 5843.24m
Limited compaction and cement free facies	Fined to medium grained, well-sorted, rare in carbonate cements	Low degree of compaction; free of cements	Both primary pores and intragranular dissolution pores	 B8, 8081.84m

characterize carbonate cement generations.

Scanning Electron Microscope (SEM) secondary electron image analysis was performed on freshly broken rock surfaces to document pore-filling cement, especially authigenic clay minerals as well as authigenic quartz cements.

We used conventional well logs including calipers (CAL), deep and shallow lateral logs (LLD, LLS), high resolution induction resistivity logs (M2R2, M2R3, M2Rx, etc), Spontaneous Potential (SP), Gamma Ray (GR), sonic transit time (AC), bulk density (DEN) and compensated neutron log (CNL). We matched core depth to well log depth by correlating distinctive features in core (mudstones layers or fractures) with conventional well logs.

We used data that was collected from 2018 to 2021 using Schlumberger's Fullbore Formation MicroImager (FMI) imaging logging tool. This tool makes a resistivity map of the borehole wall (e.g. Poppelreiter et al., 2010). Image logs were run in water-based mud. Borehole static and dynamic images were generated through speed correction, eccentricity correction, and (dynamic) normalization. Geological objects including bedding (bedding planes or crossbedding), and fractures (natural fractures and induced fractures) were manually picked on image logs (Pang et al., 2022). Image log observations combined with core data identify lithology and sedimentary structures (beds). We used the image logs to document fracture attributes including strike, dip and dip angles and used conductive or resistive characteristics of fracture traces to assess whether fractures are open or sealed (Lai et al., 2023). We term this assessment status (open or closed).

## 4. Results and discussion

### 4.1. Depositional microfacies

The lithologies of  $K_1bs_3$  member (third member of Bashijiqi Formation) consist of pebbly sandstone, or conglomerates (Fig. 2A and B), and the lithologies of  $K_1bs_2$  and  $K_1bs_1$  include sandstones (fine to

medium-grained), siltstone and mudstone (Fig. 2C, D, 2E, 2F, 2G). The pebbly sandstone or conglomerates are mainly massive without visible beds (Fig. 2A and B), while the fine to medium-grained sandstones have parallel beds, inclined beds and cross beds (tabular, wedge-shape and trough) (Fig. 2C, D, 2E). There are massive fine-medium grained sandstones (Fig. 2E). Wavy beds are present in siltstones (Fig. 2F). Mudstones are red to brown in color and generally have no visible beds (Fig. 2G). In some cases, other sedimentary structures such as scour surfaces (rapid change from mudstones into sandstones) or reactivation surfaces (rapid change from sandstones into conglomerates) can be detected (Fig. 2H and I).

Distributary channels microfacies have high depositional water energy, and mainly include sandstones (fine to medium grained) with various types of sedimentary structures (parallel bedding, or cross beds). FMI image logs confirm the presence of bedding planes, and in some cases, scour surfaces can be observed (Fig. 3). The distributary channel microfacies has a bell-shaped or box-shaped GR curve shape, indicating a fining-upward sequence or unique sequence (Zhong et al., 2003; Lai et al., 2017a). The river mouth bar microfacies have coarsening upward sequence. Therefore the GR curves generally show funnel-shaped patterns. The lithology of river mouth bar microfacies is mainly fine-grained sandstone. Bedding planes can occasionally be observed. The river mouth bar microfacies is locally distributed. The massive mudstones have high GR values, and correspond to the dark bands on the image logs (Fig. 4) (Lai et al., 2017a). The high energy distributary channel deposits were frequently blocked by distributary bay mudstones and in some cases river mouth bar sandstones (Lai et al., 2015) (Fig. 3; Fig. 4).

The sandstone rocks are mainly grain supported, and the quartz and feldspar grains are mostly moderately to well sorted, subrounded to subangular (Fig. 5) (Lai et al., 2017a).



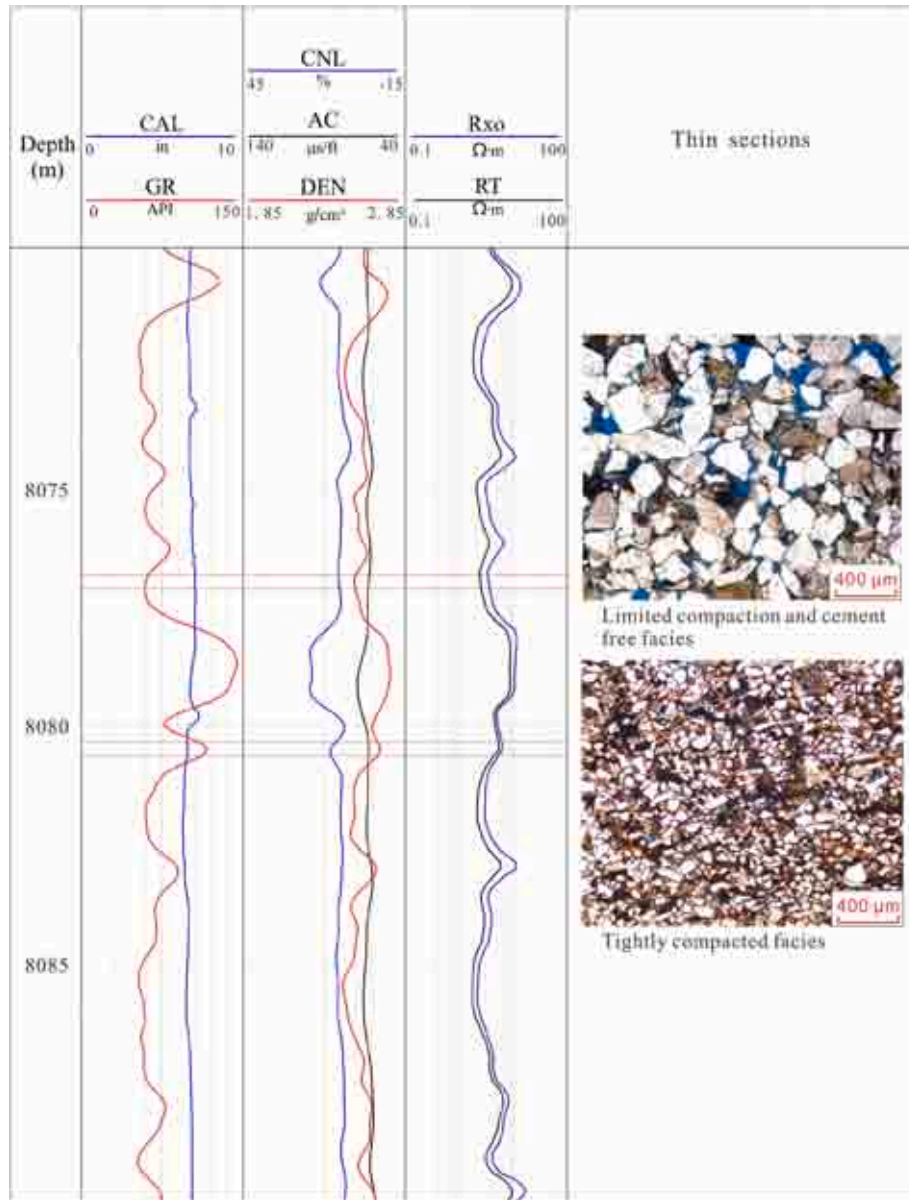


**Fig. 7.** Well log responses and thin section photo of tightly compacted facies and limited compaction and cement free facies in Bozi-Dabei wellblock of Kuqa depression

The tightly compacted facies is recognized as high GR, high density

The limited compaction and cement free is recognized as low GR, low bulk density.

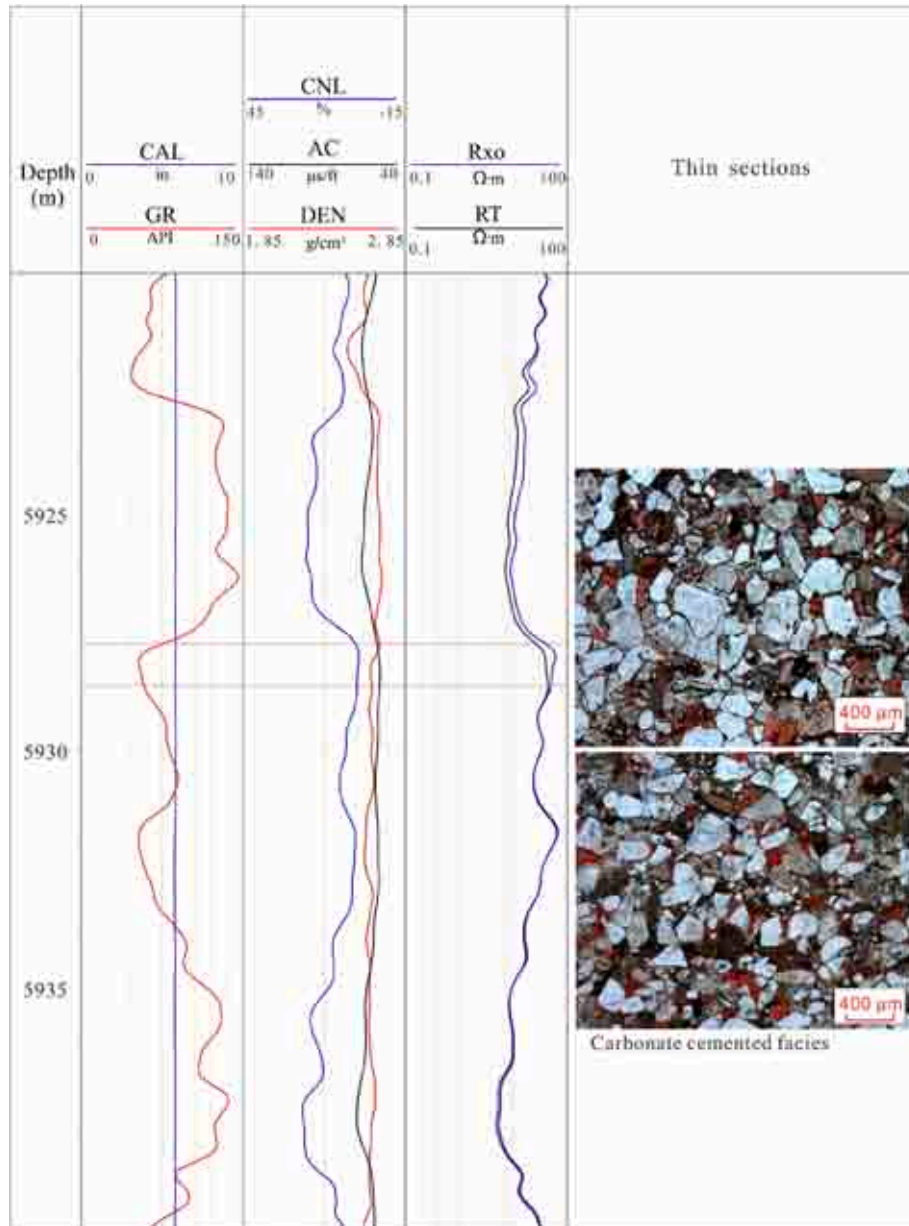


**Fig. 8.** Well log responses and thin section photo of carbonate cemented facies in Bozi-Dabei wellblock of Kuqa depression. The carbonate cemented facies is recognized as high density, high resistivity, and low GR.

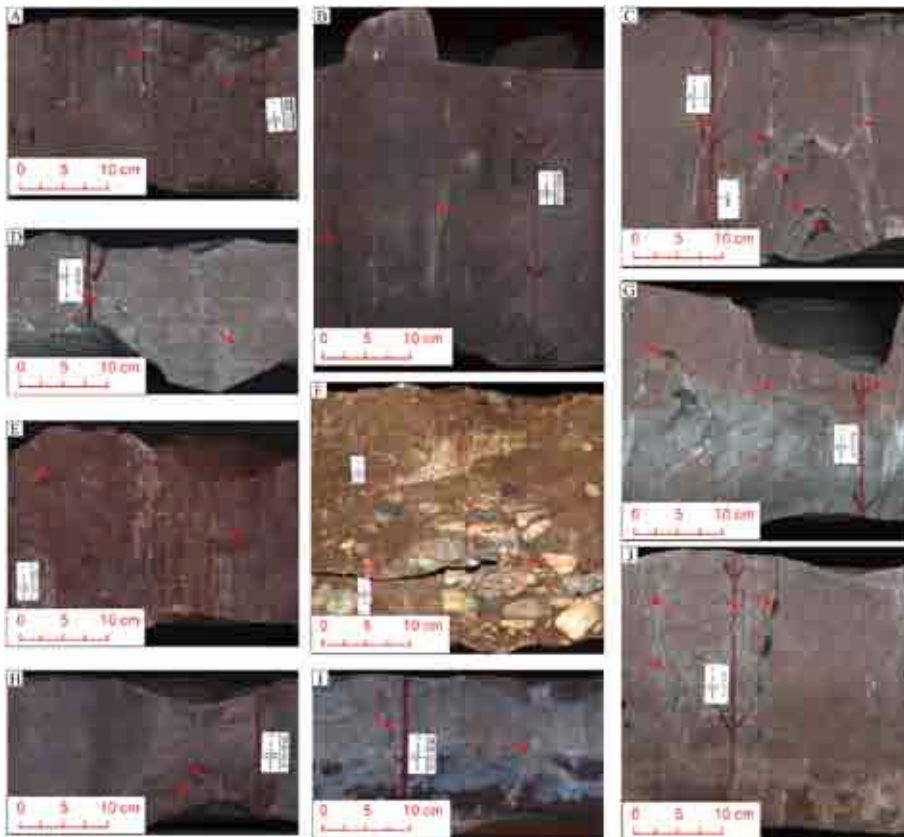


**Fig. 9.** Core photos (unfolded images) showing fractures with various attributes (dip angles) and status (open to partly open to closed) in Bozi-Dabei well-block of Kuqa depression.

- A. Vertical fracture (arrow), Well B104
- B. High angle fracture (arrow), Well B104
- C. Crosscut of high dip angle fractures (arrow), Well B301
- D. Low angle fracture (arrow), Well B301
- E. Low angle fracture (arrow), Well B12
- F. Horizontal fracture in conglomerate (arrow), Well B1
- G. Open fracture (arrow), Well B301
- H. Partly (calcite) filled fracture (arrow), Well B103
- I. Closed (calcite filled) fracture (arrow), Well B103
- J. Fracture network (arrow), Well B301.

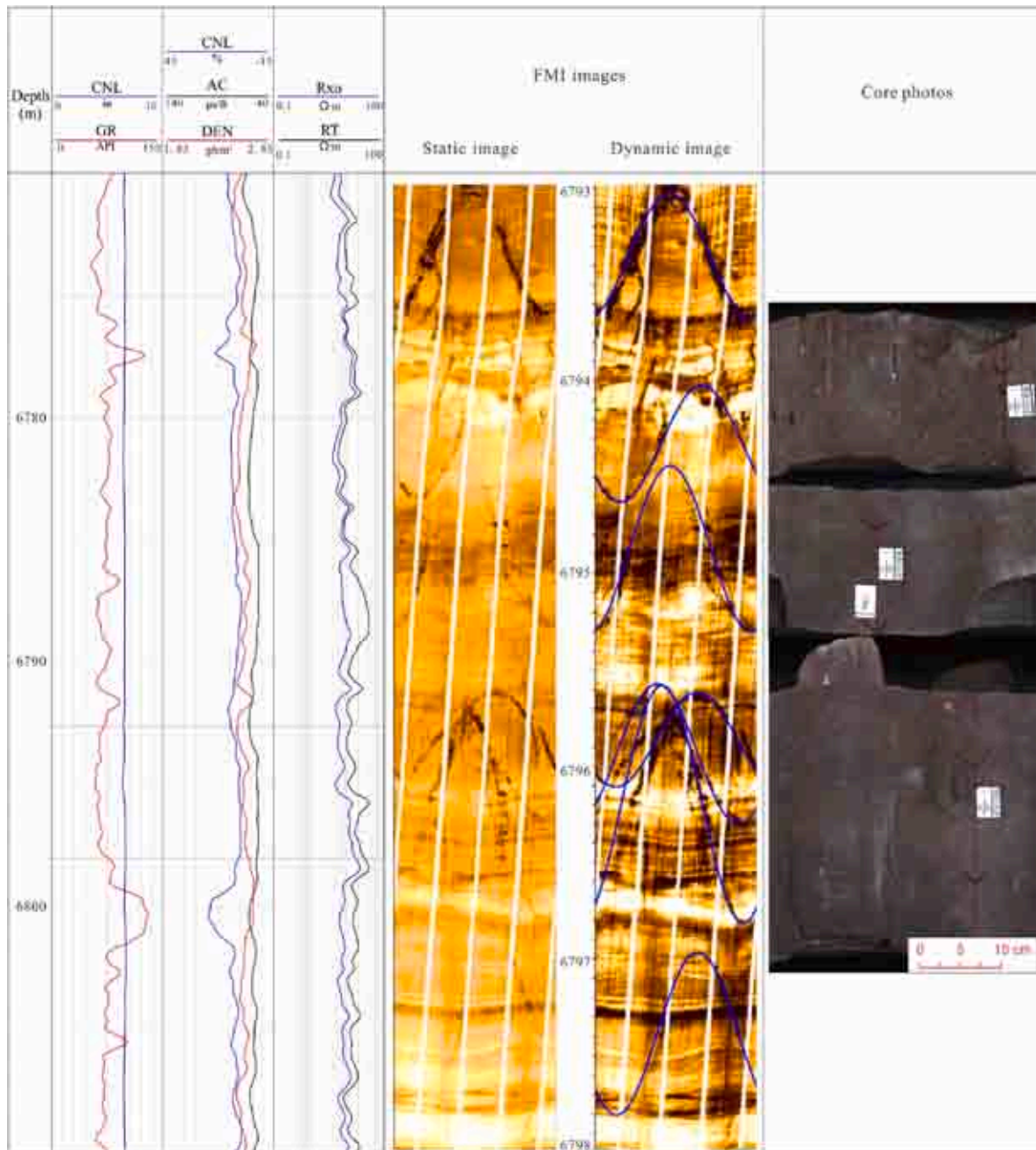


**Fig. 10.** Conventional well and image log responses of natural fractures in Bozi-Dabei wellblock of Kuqa depression. The natural fracture is recognized as dark sine waves on the image logs. Dip angle is determined by the sine wave amplitude, while dip direction can be derived from the lowest point of the sine traces.

**Table 2**  
Image log derived fracture parameters for Well B104.

Strata	Depth intervals with fractures	Open fractures		Closed fractures		Number of fracture	FVDC (1/m)		FVTL (m)		FVAH (mm)		FVPA (%)	
		Dip angles	Average dip	Dip angles	Average dip		Max	Ave	Max	Ave	Max	Ave	Max	Ave
K <sub>1</sub> bs <sub>2</sub>	6748-6760 Inclined fractures	45°–80°	72°∠45°	18°–28°	22°∠182°	13	3.2	1.5	5.2	2	7.8	4.2	0.08	0.05
	6767-6772 Inclined fractures	40°–85°	74°∠52°			6	3	1.4	4.2	2.3	9.5	4.5	0.07	0.05
	6779-6781 Inclined fractures	70°–82°	76°∠42°			4	3.5	1.4	4	2.5	5.2	3.9	0.09	0.06
	6783-6785 Inclined fractures	50°–78°	65°∠60°			12	7	5	11	6.5	5.4	4.2	0.18	0.11
	6793-6797 Inclined fractures	58°–75°	68°∠352°			8	3	1.7	5	3.4	4.3	2.9	0.09	0.06
	6802-6804 Inclined fractures	55°–68°	62°∠48°			7	5.5	4.3	5.5	4.3	5.2	4.1	0.15	0.1
	6812-6827 Inclined fractures	50°–81°	67°∠68°			23	3.1	1.4	5	2.8	8.1	4.2	0.12	0.06
K <sub>1</sub> bs <sub>3</sub>	6835-6851 Inclined fractures	70°–82°	75°∠62°			12	2.5	1.5	4	2.5	7.4	3.6	0.09	0.06
	6856-6863 Inclined fractures	51°–81°	65°∠230°			5	2.5	1.6	3	2.4	3.1	2.1	0.1	0.08
	6868-6888 Inclined fractures	55°–85°	68°∠274°			18	5.5	2.1	6	3.2	4.2	2.6	0.11	0.06
	6893-6901 Inclined fractures	40°–78°	64°∠210°			11	2.5	1.5	4.5	3.5	4.3	2.3	0.08	0.06
K <sub>1</sub> bx	6926-6929 Inclined fractures	35°–72°	52°∠312°	20°–30°	24°∠274°	9	5	3.2	5.1	3.4	2.8	1.8	0.09	0.07

## 4.2. Diagenetic facies

### 4.2.1. Diagenesis

The Bashijiqike Formation in the Bozi-Dabei wellblock have average burial depths larger than 6000 m. There are abundant intergranular pores preserved (Fig. 5A), and the point or point to line grain contacts can be observed (Fig. 5B) (Lai et al., 2022b; Xin et al., 2022).

There are grain-coating clay minerals in the form of mixed-layer illite/smectite present around the grain boundaries, and consequently quartz cementation is retarded at deep burial depth (Lai et al., 2017a). There are no evident quartz cements with the clay mineral-coated grains (Fig. 5A and B).

There are no intergranular pores observed in the very fine-grained rocks or very poorly sorted rocks (Fig. 5C and D).

Most of the pore spaces by thin section observation are primary intergranular pores, and there are grain-coating clays present, while dissolution pores are rare (Xin et al., 2022) (Fig. 5E and F). Fairly angular detrital quartz grains, and the areas of high porosity look to have abundant grain coats (Fig. 5E and F).

### 4.2.2. Diagenetic minerals

Carbonate cements are the predominant pore filling cements in these sandstones. Thin sections prove the presences of calcite (Fig. 6A), and cathode luminescence analysis confirms the presence of carbonate cements, which display bright orange to yellow luminescence color patterns (Fig. 6B). Carbonates occur as pore filling cements or in some cases replacing framework grains (feldspars) (Fig. 6B). The high intergranular volume (IGV) (intergranular pore + cement) confirms that carbonate cements are the most volumetrically important diagenetic minerals, and they greatly reduce porosity.

Gypsum deposits can be detected on SEM images (Fig. 6C). Additionally, SEM images confirm the presence of various types of clay minerals. Illite as well as mixed layered illite/smectite are predominant (Fig. 6D and E), and there are only minor amounts of quartz cement (Fig. 6E and F). Quartz cements are absent where the grain-coating clays are present (Fig. 5E and F).

### 4.2.3. Diagenetic facies and well log response

Diagenetic facies were classified by compaction state and the type and pattern of diagenetic minerals present (Lai et al., 2020; Wu et al., 2020). Here in this study, three diagenetic facies are recognized, and they include (1) tightly compacted facies, (2) carbonate cemented facies, and (3) limited compaction and cement free facies (limited compaction and lacking cement). Each diagenetic facies have their varied diagenetic degree, diagenetic minerals and individual pore spaces (Table 1).

The limited compaction and cement free diagenetic facies has a limited (relatively low) degree of compaction (IGV from 15% to 25%), and the content of cement especially the carbonate and quartz cements is very low (0–3%). However, this facies contains grain-coating clay minerals that help preserve intergranular pores (Lai et al., 2017a). The high energy depositional facies has fine to medium grain size and well sorted framework grains, and thus minimal compaction (IGV ca. 20%) (Table 1). Additionally, there are no cements filling in the pore spaces. Consequently, pore spaces, especially large intergranular pores, can be preserved. Therefore this type of diagenetic facies has the highest porosity. Here thin section observation confirms both intergranular pores and intragranular dissolution pores (Table 1). All three porosity curves (low bulk density <2.55 g/cm<sup>3</sup>, high CNL value > 10%, and high sonic transit time >60 μs/ft or 197 μs/m) give the signature of relatively high reservoir quality. In addition, the limited compaction and cement free facies has a low GR reading (<60 API), indicating a matrix free and high energy depositional microfacies (Fig. 7).

The tightly compacted diagenetic facies is mainly associated with intervals rich in detrital clays or ductile rock fragments, or those very fine grained or very poorly sorted successions, which are easily compacted during deep burial (Table 1). Consequently, tightly compacted facies are recognized on well logs by their high bulk density (>2.6 g/cm<sup>3</sup>). The abundance of detrital clays or very fine grain size results in a relatively high GR reading (>60 API) (Cui et al., 2017; Lai et al., 2018) (Fig. 7). Additionally, resistivity values are reduced due to abundance of ductile detrital clay. However, CNL and AC curves may give apparent high porosity values (high CNL and high AC values) (Fig. 7).

The carbonate cemented diagenetic facies is associated with fine to medium-grained sandstones, which are matrix free. The dominance of carbonate cements and very high IGV locally result in a floating texture

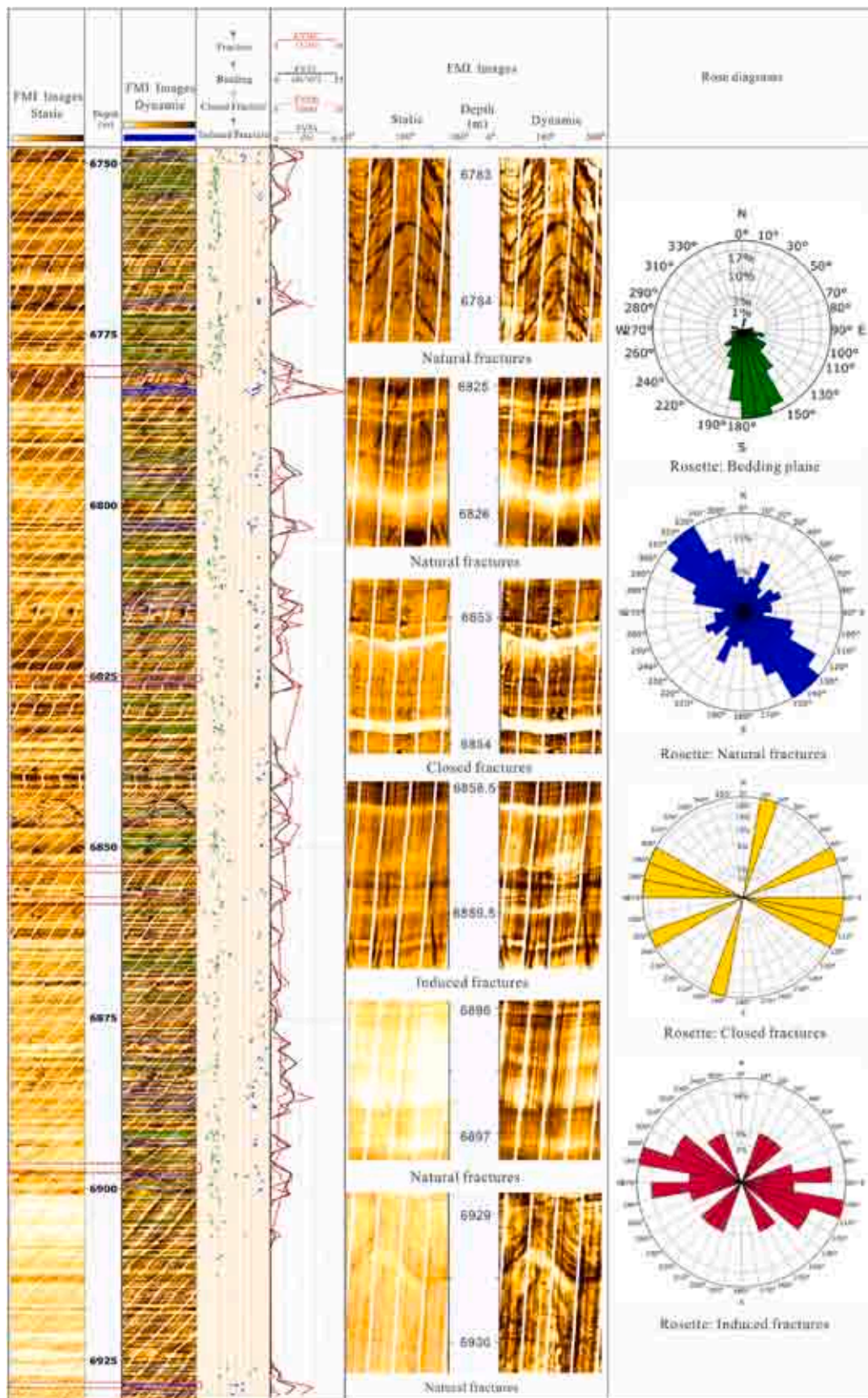


**Fig. 11.** Comprehensive evaluation of natural fractures, induced fractures and fracture effectiveness using image logs for Well B104. A total of 128 natural (open) fractures are recognized as blue sine waves, and the rose diagrams show a dominant NW-SE strike, and there are 10 filled fractures picked as yellow. The induced fractures are picked as red, showing a near W-E direction. (For interpretation of the references to color in this figure legend, the reader is referred to the Web version of this article.)

**Table 3**  
Oil test data of the three wells in Figs. 12, 13 and 15.

Well Name	Depth intervals (m)	Choke width (mm)	Daily oil productivity (m <sup>3</sup> )	Daily natural gas production (m <sup>3</sup> )	Drawdown pressure (MPa)
B104	6757–6850	7.0	38.9	516369	80.4
B22	6267–6387	6.0	/	7588	10.0
B302	6185.5–6197.5	5.0	40.38m <sup>3</sup>	207166	70.0

(Table 1). Therefore, carbonate cemented facies are easily recognized on well logs by their low GR values (<60 API), low AC values (<60  $\mu\text{s}/\text{ft}$ ), low CNL porosity (<10%) but high bulk density (>2.6 g/cm<sup>3</sup>) and high resistivity readings (>20  $\Omega\text{ m}$ ) (Fig. 8) (e.g., Ozkan et al., 2011; Lai et al., 2018; Lai et al., 2020). Both tightly compacted and carbonate cemented diagenetic facies have porosity in the range of 1.5%–4.5%.

#### 4.3. Fractures

##### 4.3.1. Fracture observations

Core observations show that fractures in the Bashijiqike and Baxigai Formation have a wide range of dip angles (and strikes) and degree of fill (Fig. 9). There are vertical fractures and high dip angle fractures (>60°) (Fig. 9A, B, 9C), medium dip angle fractures (30°–60°) (Fig. 9D), and low angle fractures (<30°) (Fig. 9E) as well as horizontal fractures (Fig. 9F). High dip angles fractures crosscut each other (Fig. 9C). Additionally fractures can be classified into (1) open fractures (Fig. 9G), (2) partially open fractures (Fig. 9H), and (3) closed fractures (Fig. 9I).

In some cases, the fractures with various status (open to partly open to closed) and attributes (dip angles) can constitute a well-connected fracture network (dense, interconnected fracture traces at the core scale) (Fig. 9I), and enlargement along fracture surfaces can be observed (Fig. 9J). Fractures occur in the fine-medium grained sandstone or the conglomerates, while fractures in mudstones are rare (Fig. 9). The cements filling the fracture are mainly calcites (Fig. 6B) (Lai et al., 2022b).

##### 4.3.2. Fracture detection using well logs

In water-based mud drilled wells, closed or open fractures can be easily picked out on FMI image logs as resistive or conductive linear anomalies (Fig. 10) (Ameen et al., 2012; Lai et al., 2019). Fractures are divided into artificial (drilling induced) and natural fractures based primarily on configuration patterns according to standard procedures, and the latter can be further classified into filled or unfilled (open) fractures according to filling degree inferred from resistive or conductive character (Lai et al., 2017b). Natural open inclined fracture traces show dark continuous sinusoidal waves on image logs (Lai et al., 2022c). Dip angles can be determined by the sine wave amplitude, and dip direction can be derived from the lowest point of the sine traces (Fig. 10) (Nie et al., 2013). In addition, the partly to fully closed fractures manifest as discontinuous or continuous bright-dark sinusoidal traces (Fig. 10). Where fracture surfaces are fully filled by resistive minerals (calcite), bright sinusoidal wave traces are encountered (e.g., Khoshbakht et al., 2009). Therefore both fracture attributes (dip angles) and status (open, sealed) can be determined from image logs (e.g., Lai et al., 2021).

In addition, from image logs we derive parameters including fracture porosity (FVPA), aperture (FVAH), length (FVTL) and density (FVDC) (Table 2). Length is usually a partial measure of fracture height that is severely censored by the limited intersection with the wellbore. Fracture parameters for each depth intervals are summarized in Table 2.

Based on induced fractures of Well B104 (Fig. 11), maximum horizontal stress ( $SH_{\text{max}}$ ) orientation is determined as having dominantly an east-west trend (100°–110°). Open fractures are dominated by NW-SE strike (120°–150°) as documented on the strike composite rose diagram. Additionally, closed fractures have three dominant strikes as

indicated on the rose diagram. Open fractures are not parallel to  $SH_{\text{max}}$  but have strike divergence of less than 30° with respect to  $SH_{\text{max}}$  (Fig. 11).

Depositional microfacies controls lithology and sandstone composition and texture, and facies plays the first role in determining porosity. Most pore spaces in sandstones are facies controlled or environment selective, and the high energy depositional microfacies (distributary channel microfacies) control the porosity in sandstones (Bjørlykke, 2014; Lai et al., 2017a).

In addition to depositional facies and initial sediment composition, subsequent burial diagenetic alterations modify porosity (Nygard et al., 2004; Mansurbeg et al., 2008; Ozkan et al., 2011; Lai et al., 2022c). Though in high energy depositional facies (distributary channel microfacies), diagenetic modifications vary greatly, and this will lead to a large variation in reservoir quality (Morad et al., 2010; Lai et al., 2013, 2018). Therefore high energy depositional microfacies plays a primary role in controlling reservoir quality, however, in certain depositional microfacies, the final reservoir quality is determined by the late-stage diagenetic modifications or the presence of fractures. Especially, in tight sandstones, diagenesis and diagenetic minerals exert important controls on improving, preserving, or destroying reservoir quality (Salem et al., 2005; Lai et al., 2013; Zhang et al., 2015; Becker et al., 2017). For instance, compaction will be extensive in rocks where ductile grains such as soft volcanic rock fragments or detrital clays are abundant or the framework grains are fine or are poorly sorted (Fig. 5C and D) (Rossi et al., 2001; Weber and Ricken, 2005; Cao et al., 2017).

The degree of compaction is variable due to complexity of detrital mineralogy and texture (Tobin et al., 2010). Compaction is more extensive in rocks abundant with detrital clays or argillaceous fragments (Paxton et al., 2002; Morad et al., 2010; Ozkan et al., 2011; Lai et al., 2016). Detrital clay-rich successions or very fine-grained layers are more tightly compacted than those abundant in rigid grains (Weber and Ricken, 2005; Bjørlykke and Jahren, 2012), especially for the Bashijiqike and Baxigai Formations which are ultra-deeply buried to >7 km (Lai et al., 2017a). The presence of grain-coating clays helps preserve intergranular pore spaces by inhibiting quartz cements.

Tight sandstones have low matrix porosity (<10%), therefore they require the development of natural fractures to allow oil and gas flow to the wellbore (Laubach, 2003; Ameen et al., 2012; Khoshbakht et al., 2012; Lai et al., 2017b, 2021). Fractures are important fluid-flow conduits and hydrocarbon repositories in the subsurface (Zeng, 2010). The presences of fractures in tight sandstones will significantly improve permeability and hence reservoir performance (Nelson, 2001; Ameen and Hailwood, 2008; Nian et al., 2021).

#### 4.4. Reservoir quality and productivity evaluation

##### 4.4.1. Hydrocarbon productivity

The Well B104, of which the image log interpreted fractures are presented in Fig. 11, contains abundant fractures, and Well B104 has obtained high oil and gas productivity. The oil test reveals that in the 6757–6850 m depth intervals of B104, the daily oil production is 38.9 m<sup>3</sup>, and the daily natural gas production is 516369 m<sup>3</sup> with 7 mm choke width and drawdown pressure of 80.495 MPa (Table 3). Additionally, when interpreting the matrix porosity in terms of depositional microfacies and diagenetic facies, it is found that the depositional microfacies is mainly distributary channel facies and the diagenetic facies is dominantly of limited compaction and cement free facies (Fig. 12). The GR curves mainly display box-shape, representing a high depositional energy, and the related image logs confirm that. As can be observed from the image logs, abundant cross beddings and parallel bedding are detected, which implies the high energy of depositional microfacies (Fig. 12). The sandstones in this depth interval are therefore mainly matrix-free sandstones (fine-medium grained) with cross beds, and therefore are favorable for formation of high-quality reservoirs (Fig. 12). In addition, the thin sections unravel the intergranular and intragranular

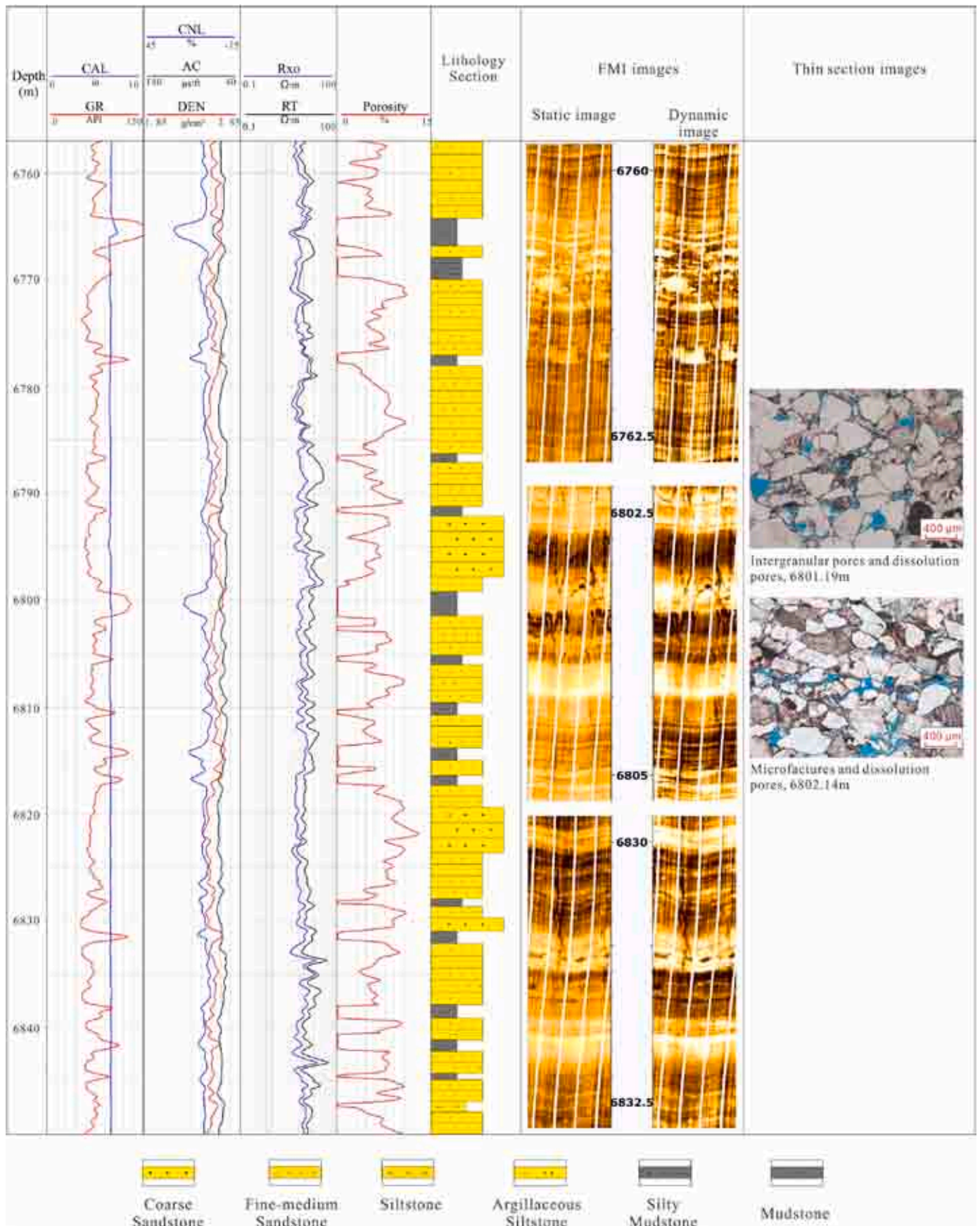


Fig. 12. Interpretation of depositional microfacies and diagenetic facies for Well B104.



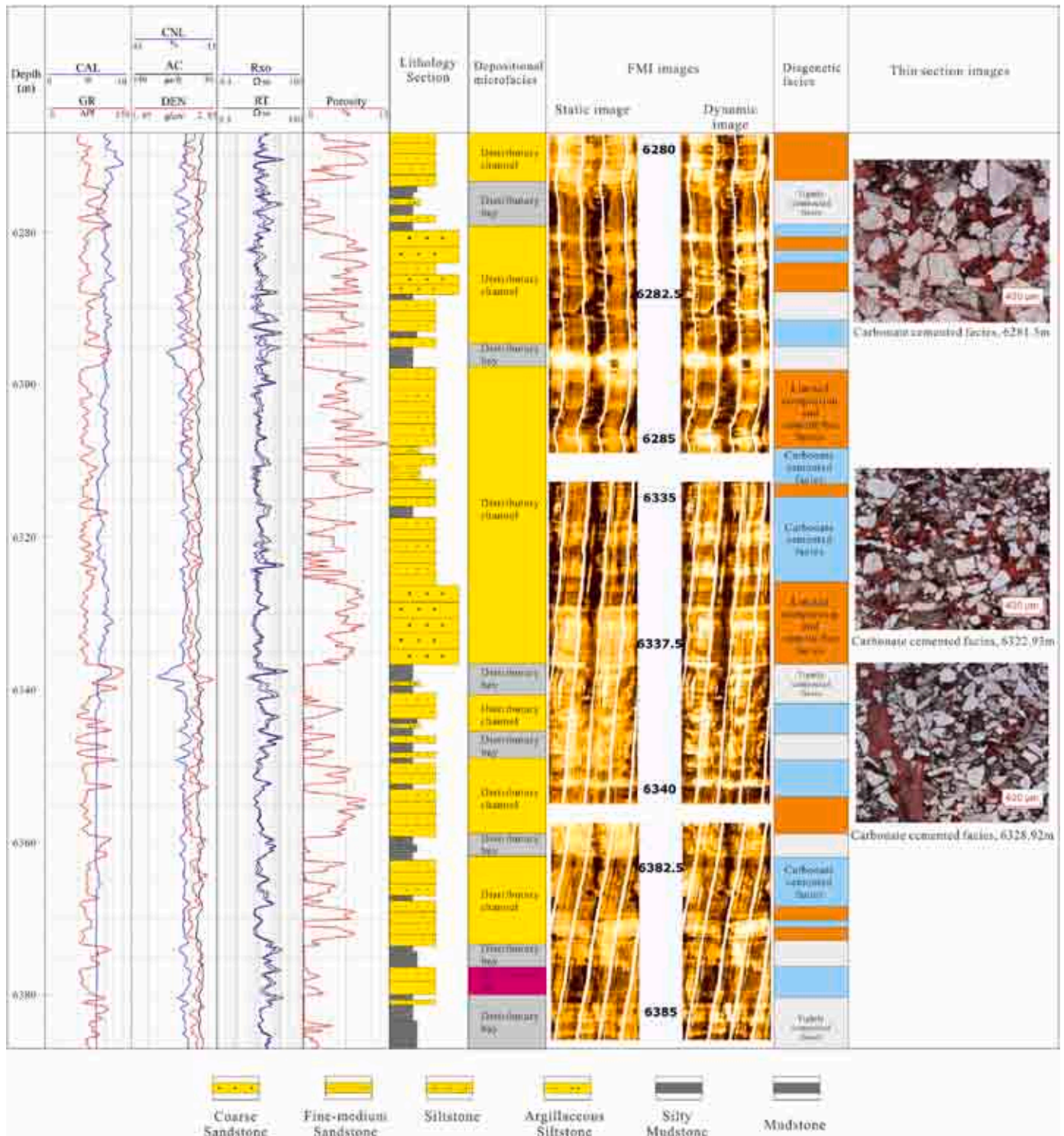


Fig. 13. Interpretation of depositional microfacies and diagenetic facies for Well B22.

pore spaces in the sandstones, and the grains are mainly fine-medium grained with low matrix content, which also represents a high depositional energy, and there are no evident carbonate cements filling the pore spaces (Fig. 12). The diagenetic facies is therefore determined as limited compaction and cement free facies.

4.4.2. Reservoir quality evaluation and prediction

Despite the great depth of these rocks, depositional facies and original grain content and grain size remain an important determinant of

porosity. The Well B22 is dominantly of high energy distributary channel microfacies, as can be confirmed by the box- or bell shape GR curves (Fig. 13). Though deposited in high energy microfacies, the diagenetic facies is mainly carbonate cemented facies as interpreted from thin section observations. Therefore the matrix porosity is low due to the distributary channel microfacies sandbodies are tightly cemented by carbonates (Fig. 13). The extensive carbonate cements will greatly reduce the matrix porosity (Mansurbeg et al., 2008; Dutton and Loucks, 2010). In addition, it is found that there are only minor fractures

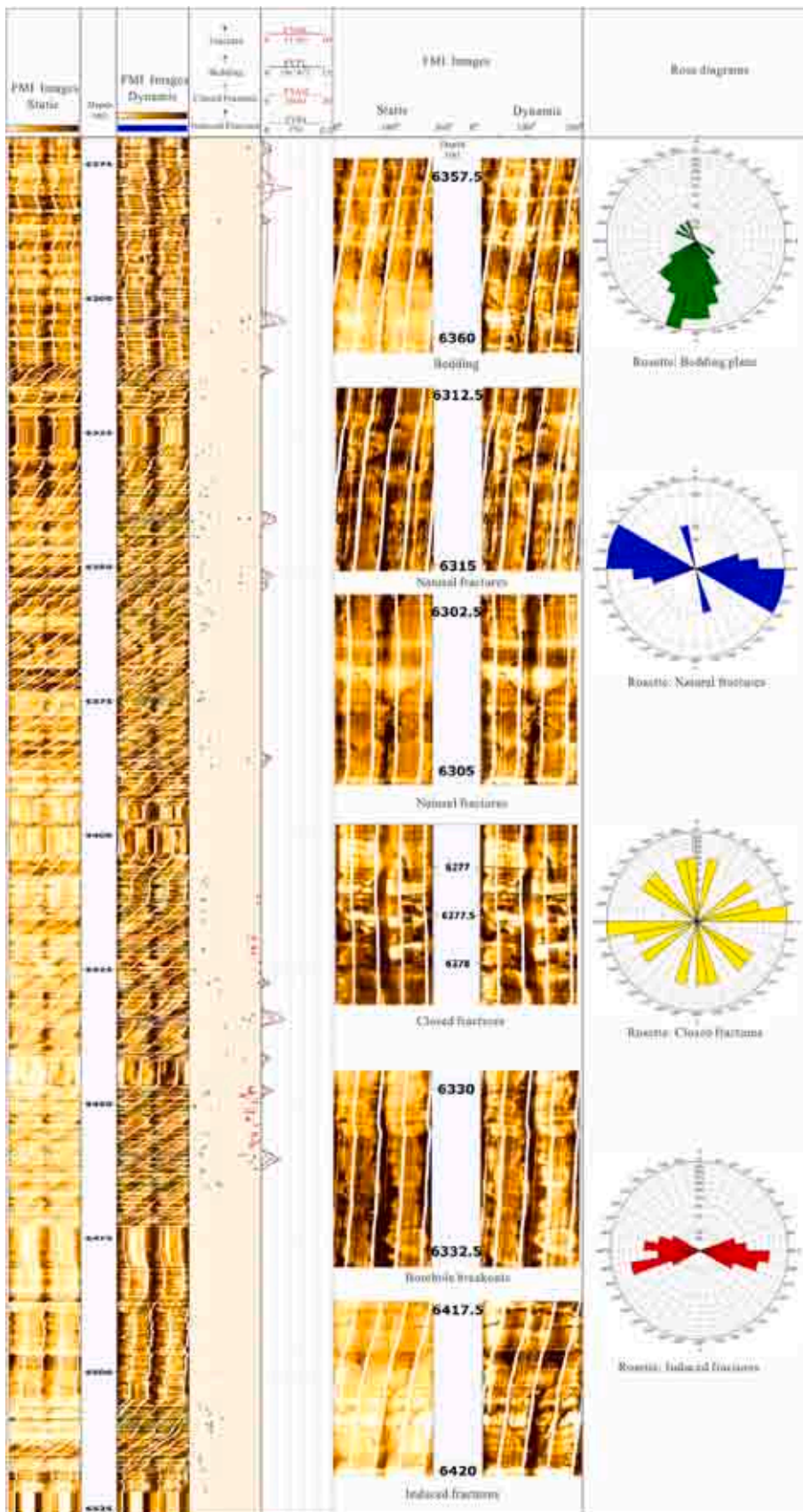


**Fig. 14.** Comprehensive evaluation of natural fractures, induced fractures and fracture effectiveness using image logs for Well B22. Fracture attributes and status are picked by image logs, natural fractures are recognized as blue sine waves, and the rose diagrams show a dominant NW-SE strike, and there are many sets of filled fractures picked as yellow. The induced fractures are picked as red, and show a E-W direction. (For interpretation of the references to color in this figure legend, the reader is referred to the Web version of this article.)

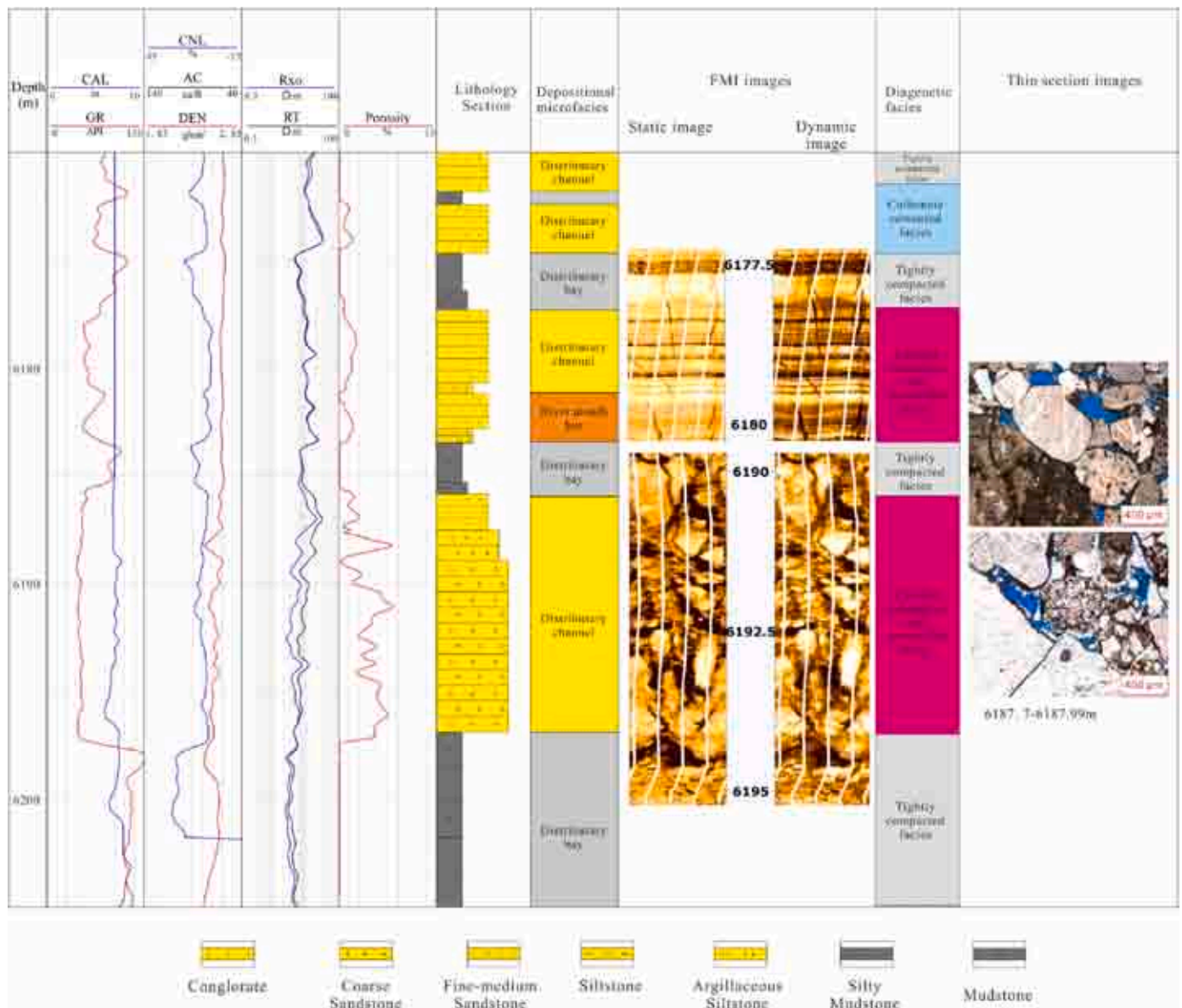


Fig. 15. Interpretation of depositional microfacies and diagenetic facies for Well B302.

detected when interpreting fractures using image logs. Most of the distributary channel microfacies sandbodies contain no fractures (Fig. 14). Therefore it can be concluded that Well B22 has low reservoir quality and low hydrocarbon productivity from the aspect of depositional microfacies, diagenetic facies and fractures (Figs. 13 and 14). In the 6267–6387 m depth intervals of Well B22, the oil test reveals that only 7588 m<sup>3</sup> daily natural gas productivity is obtained with 6 mm choke width and drawdown pressure of 9.959 MPa (Table 3).

The Well B302 is dominantly deposited in high energy facies, and the microfacies is dominantly distributary channel microfacies. The box-or bell shape GR curves as well as the cross beddings interpreted from image logs support that the sandbodies are deposited in high energy environments (Fig. 15). In some layers, the lithology is conglomerate, which also represent a high energy depositional facies (Fig. 15). From the aspect of thin section interpreted diagenetic facies, it is found that the intergranular pores are common, and dissolution can occur along the intergranular pore spaces. Additionally, there are no carbonate cements and the matrix is rare, therefore the diagenetic facies is interpreted as limited compaction and cement free facies (Fig. 15). Consequently, the depositional microfacies and diagenetic facies support high matrix

reservoir quality of Well B302 (Fig. 15). Image log fracture observations show that fractures are abundant in the Well B302, most of the distributary channel microfacies sandbodies are highly fractured, and even in conglomerates, the fractures are commonly detected (Fig. 16). In some interpretation intervals, the fracture density (FVDC) can reach as much as 10 per meter, and the fracture aperture can reach as high as 20 mm (Fig. 16). Therefore it can be concluded that the Well B302 has both high matrix reservoir quality and high hydrocarbon productivity from the aspect of depositional microfacies, diagenetic facies and fractures (Figs. 15 and 16). In the 6185.5–6197.5 m depth intervals of Well B302, the oil test has obtained a high hydrocarbon productivity. The daily oil production is 40.38 m<sup>3</sup>, and the daily natural gas production is 207166 m<sup>3</sup> with 5m choke width and drawdown pressure of 69.651 MPa (Figs. 15 and 16) (Table 3).

The combination of low energy distributary bay microfacies, tightly compacted (or carbonate cemented) diagenetic facies and no fracture has no hydrocarbon productivity. The combination of high energy distributary channel depositional microfacies, limited compaction and cement free diagenetic facies but no fracture will result in a low hydrocarbon productivity (Fig. 17). Further, the combination of

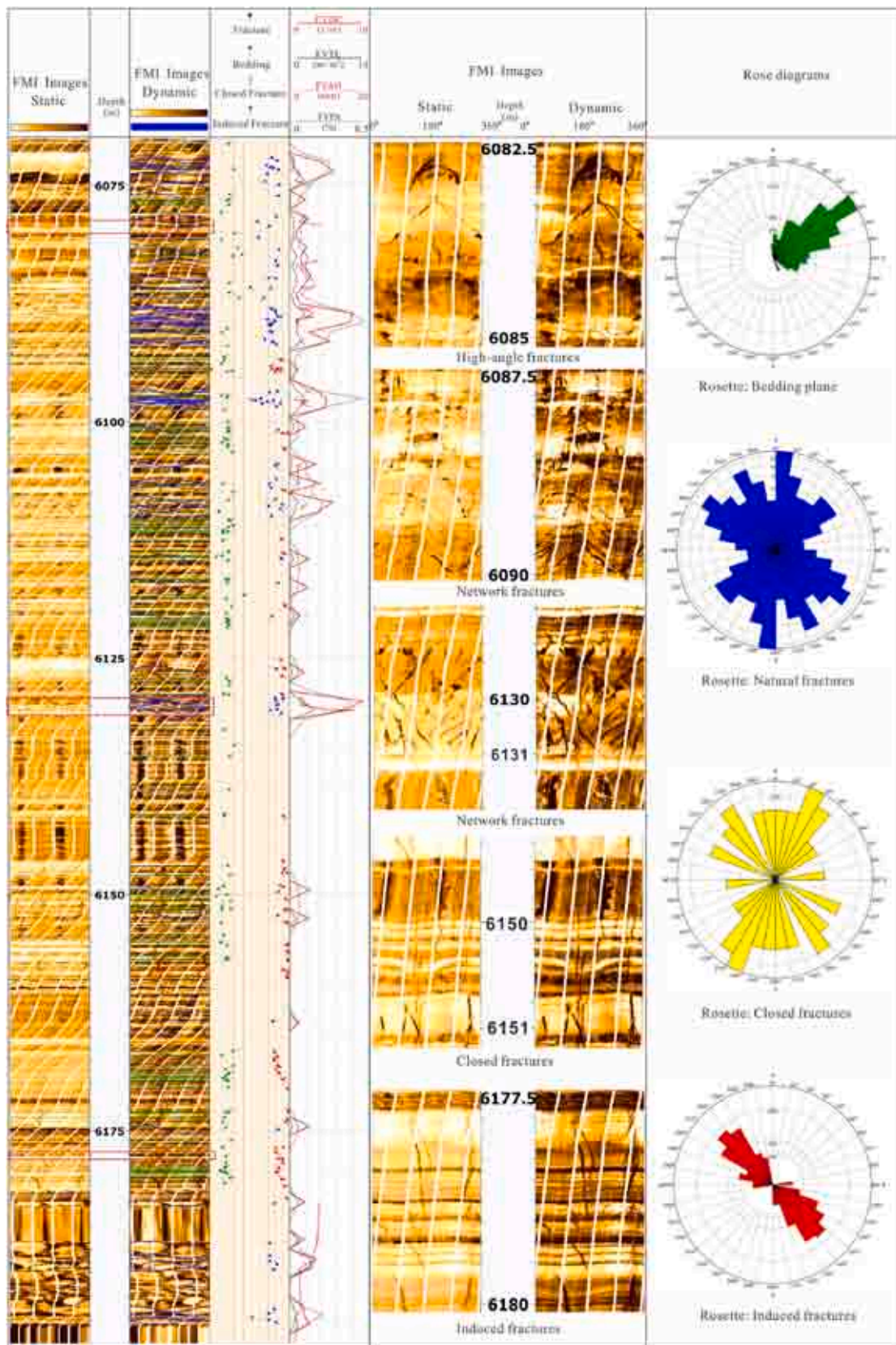


**Fig. 16.** Comprehensive evaluation of natural fractures, induced fractures and fracture effectiveness using image logs for Well B302. Fracture attributes and status are picked by image logs, natural fractures are recognized as blue sine waves, and the rose diagrams show four sets of strike, and there are many closed fractures picked as yellow. The induced fractures are picked as red, and show a NW-SE direction. (For interpretation of the references to color in this figure legend, the reader is referred to the Web version of this article.)

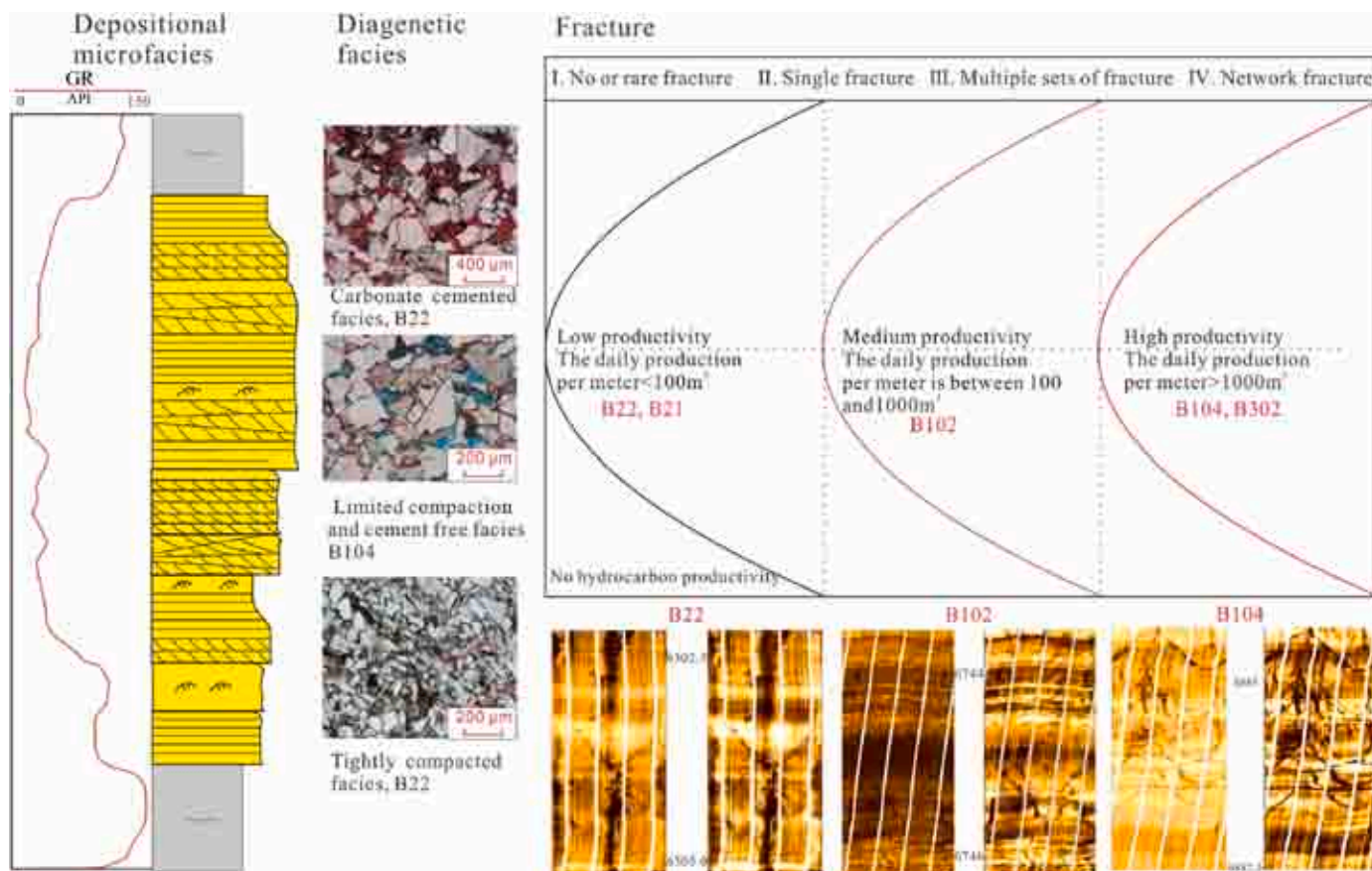


Fig. 17. Coupling relationships between hydrocarbon productivity and depositional microfacies, diagenetic facies and fractures.

distributary channel microfacies, limited compaction and cement free diagenetic facies and network fracture will contribute to the highest hydrocarbon productivity (Fig. 17). Additionally, the degree of fracture developments (ranging from I. Rare fracture, II. Single fracture, III. Multiple sets of fractures, to IV. Network fractures) as well as the depositional and diagenetic facies determine the reservoir quality (Fig. 17).

## 5. Conclusions

Although Cretaceous sandstones of Kuqa depression are at depths of ca. 8000 m, they retain primary and secondary porosity, and open fractures. Depositional microfacies, diagenetic facies as well as fracture determine the reservoir quality.

Depositional microfacies include distributary channel, mouth bar and distributary bay as well as lacustrine microfacies that experienced low to medium mechanical compaction. Calcite is the dominant diagenetic mineral. Pore spaces are dominantly intergranular, but the intensity of dissolution is low.

Diagenetic facies are divided into tightly compacted facies, carbonate cemented facies, and limited compaction and cement free facies. The limited compaction and cement free diagenetic facies is characterized by low GR reading, low bulk density, high CNL value, and high sonic transit time. Tightly compacted diagenetic facies is recognized on the well logs as high GR readings, high bulk density but low resistivity values. Carbonate cemented diagenetic facies is easily to be recognized as low GR values, low AC value, low CNL porosity but high bulk density and high resistivity readings.

In terms of fracture attributes and status, there are vertical opening-mode fractures and high angle fractures, medium angle fractures, and low angle fracture as well as horizontal fractures. Reservoir quality and

hydrocarbon productivity are evaluated by superposing depositional microfacies, diagenetic facies and fracture. Depositional microfacies and diagenetic facies determine the initial intergranular pores and subsequent diagenesis modified secondary pore spaces. Reservoir quality can be predicted by integrating depositional microfacies, diagenetic facies and fracture in ultra-deep sandstones.

## Author contribution statement

**Jin Lai, Dong Li and Guiwen Wang:** Conceptualization, Methodology, Software, **Fei Zhao, Tianyu Bai, Yong Ai, Hongkun Liu and Deyang Cai:** Data curation, Writing- Original draft preparation., **Kangjun Chen, Yuqiang Xie:** Visualization, Investigation., **Jin Lai, Guiwen Wang:** Software, Validation., **Jin Lai, Guiwen Wang, Fei Zhao:** Writing- Reviewing and Editing.

## Declaration of competing interest

The authors declare that they have no known competing financial interests or personal relationships that could have appeared to influence the work reported in this paper.

## Data availability

Data will be made available on request.

## Acknowledgments

This work was supported by National Natural Science Foundation of China (No. 41872133), and Science Foundation of China University of Petroleum, Beijing (No. 2462021YXZZ003) and strategic cooperation

project of PetroChina and CUPB (ZLZX2020-01-05). We thank Dr. Stephen Laubach and András Fall for their tireless editing on my manuscript, which improve the quality of our study significantly. We also benefit from constructive comments of three anonymous reviewers.

## References

- Ajdukiewicz, J.M., Lander, R.H., 2010. Sandstone reservoir quality prediction: the state of the art. *AAPG (Am. Assoc. Pet. Geol.) Bull.* 94 (8), 1083–1091.
- Almansour, A., Laubach, S.E., Bickel, J.E., Schultz, R.A., 2020. Value of Information analysis of a fracture prediction method. *SPE Reservoir Eval. Eng.* 23 (3), 811–823.
- Ameen, M.S., Hailwood, E.A., 2008. A new technology for the characterization of microfractured reservoirs (test case: Unayzah reservoir, Wudayhi field, Saudi Arabia). *AAPG (Am. Assoc. Pet. Geol.) Bull.* 92 (1), 31–52.
- Ameen, M.S., MacPherson, K., Al-Marhoon, M.I., Rahim, Z., 2012. Diverse fracture properties and their impact on performance in conventional and tight-gas reservoirs, Saudi Arabia: the Unayzah, South Haradh case study. *AAPG (Am. Assoc. Pet. Geol.) Bull.* 96 (3), 459–492.
- Becker, I., Wüstefeld, P., Koehrer, B., Felder, M., Hilgers, C., 2017. Porosity and permeability variations in a tight gas sandstone reservoir analogue, Westphalian D, Lower Saxony Basin, NW Germany: influence of depositional setting and diagenesis. *J. Petrol. Geol.* 40 (4), 363–389.
- Bjørlykke, K., 2014. Relationships between depositional environments, burial history and rock properties. Some principal aspects of diagenetic process in sedimentary basins. *Sediment. Geol.* 301, 1–14.
- Bjørlykke, K., Jahren, J., 2012. Open or closed geochemical systems during diagenesis in sedimentary basins: constraints on mass transfer during diagenesis and the prediction of porosity in sandstone and carbonate reservoirs. *AAPG (Am. Assoc. Pet. Geol.) Bull.* 96 (12), 2193–2214.
- Busch, B., Okamoto, A., Garbev, K., Hilgers, C., 2021. Experimental fracture sealing in reservoir sandstones and its relation to rock texture. *J. Struct. Geol.* 153, 104447.
- Cao, B., Luo, X., Zhang, L., Sui, F., Lin, H., Lei, Y., 2017. Diagenetic evolution of deep sandstones and multiple-stage oil entrapment: a case study from the Lower Jurassic Sangonghe Formation in the Fukang Sag, Central Junggar basin (NW China). *J. Petrol. Sci. Eng.* 152, 136–155.
- Cui, Y., Wang, G., Jones, S.J., Zhou, Z., Ran, Y., Lai, J., Li, R., Deng, L., 2017. Prediction of diagenetic facies using well logs – a case study from the Upper Triassic Yanchang Formation, Ordos Basin, China. *Mar. Petrol. Geol.* 81, 50–65.
- Dutton, S.P., Loucks, R.G., 2010. Diagenetic controls on evolution of porosity and permeability in lower Tertiary Wilcox sandstones from shallow to ultradeep (200–6700 m) burial, Gulf of Mexico Basin, USA. *Mar. Petrol. Geol.* 27 (1), 69–81.
- Dutton, S.P., Clift, S.J., Hamilton, D.S., Hamlin, H.S., Hentz, T.F., Howard, W.E., Akhter, M.S., Laubach, S.E., 1993. Major Low-Permeability-Sandstone Gas Reservoirs In The Continental United States, p. 221. The University of Texas at Austin, Bureau of Economic Geology Report of Investigations No. 211.
- El Sawy, M.Z., Abuhagaza, A.A., Nabawy, B.S., Lashin, A., 2020. Rock typing and hydraulic flow units as a successful tool for reservoir characterization of Bentiu-Abu Gabra sequence, Muglad basin, southwest Sudan. *J. Afr. Earth Sci.* 171, 103961.
- Feng, J., Ren, Q., Xu, K., 2018. Quantitative prediction of fracture distribution using geomechanical method within Kuqa Depression, Tarim Basin, NW China. *J. Petrol. Sci. Eng.* 162, 22–34.
- Higgs, K.E., Crouch, E.M., Raine, J.I., 2017. An interdisciplinary approach to reservoir characterisation; an example from the early to middle Eocene Kaimiro Formation, Taranaki Basin, New Zealand. *Mar. Petrol. Geol.* 86, 111–139.
- Holditch, S.A., 2006. Tight gas sands. *J. Petrol. Technol.* 58 (6), 86–93.
- Jin, Z.J., Yang, M.H., Lu, X.X., Sun, D.S., Tang, X., Peng, G.X., Lei, G.L., 2008. The tectonics and petroleum system of the Qilutagh fold and thrust belt, northern Tarim basin, NW China. *Mar. Petrol. Geol.* 25, 767–777.
- Ju, W., Wang, K., 2018. A preliminary study of the present-day in-situ stress state in the Ahe tight gas reservoir, Dibe Gasfield, Kuqa Depression. *Mar. Petrol. Geol.* 96, 154–165.
- Khosbakhth, F., Memarian, H., Mohammadnia, M., 2009. Comparison of Asmari, Pabdeh and Gurpi formation's fractures, derived from image log. *J. Petrol. Sci. Eng.* 67, 65–74.
- Khosbakhth, F., Azizzadeh, M., Memarian, H., Nourozi, G.H., Moallemi, S.A., 2012. Comparison of electrical image log with core in a fractured carbonate reservoir. *J. Petrol. Sci. Eng.* 86 (87), 289–296.
- Lai, J., Wang, G., Chen, M., Wang, S., Chai, Y., Cai, C., Li, J., Zhang, Y., 2013. Pore structures evaluation of low permeability clastic reservoirs based on petrophysical facies: a case study on Chang 8 reservoir in the Jiyuan region, Ordos Basin. *Petrol. Explor. Dev.* 40 (5), 566–573.
- Lai, J., Wang, G., Chai, Y., Ran, Y., Zhang, X., 2015. Depositional and diagenetic controls on reservoir pore structure of tight gas sandstones: evidence from lower cretaceous Bashijiqike Formation in Kelasu thrust belts, Kuqa depression in Tarim Basin of West China. *Resour. Geol.* 65 (2), 55–75.
- Lai, J., Wang, G., Ran, Y., Zhou, Z., Cui, Y., 2016. Impact of diagenesis on the reservoir quality of tight oil sandstones: the case of Upper Triassic Yanchang Formation Chang 7 oil layers in Ordos Basin, China. *J. Petrol. Sci. Eng.* 145, 54–65.
- Lai, J., Wang, G., Chai, Y., Xin, Y., Wu, Q., Zhang, X., Sun, Y., 2017a. Deep burial diagenesis and reservoir quality evolution of high-temperature, high-pressure sandstones: examples from Lower Cretaceous Bashijiqike Formation in Keshen area, Kuqa depression, Tarim basin of China. *AAPG (Am. Assoc. Pet. Geol.) Bull.* 101 (6), 829–862.
- Lai, J., Wang, G., Fan, Z., Wang, Z., Chen, J., Zhou, Z., Wang, S., Xiao, C., 2017b. Fracture detection in oil-based drilling mud using a combination of borehole image and sonic logs. *Mar. Petrol. Geol.* 84, 195–214.
- Lai, J., Wang, G., Wang, S., Cao, J., Li, M., Pang, X., Zhou, Z., Fan, X., Dai, Q., Yang, L., He, Z., Qin, Z., 2018. Review of diagenetic facies in tight sandstones: diagenesis, diagenetic minerals, and prediction via well logs. *Earth Sci. Rev.* 185, 234–258.
- Lai, J., Li, D., Wang, G., Xiao, C., Hao, X., Luo, Q., Lai, L., Qin, Z., 2019. Earth stress and reservoir quality evaluation in high and steep structure: the Lower Cretaceous in the Kuqa Depression, Tarim Basin, China. *Mar. Petrol. Geol.* 101, 43–54.
- Lai, J., Fan, X., Liu, B., Pang, X., Zhu, S., Xie, W., Wang, G., 2020. Qualitative and quantitative prediction of diagenetic facies via well logs. *Mar. Petrol. Geol.* 120, 104486.
- Lai, J., Liu, S., Xin, Y., Wang, S., Xiao, C., Song, Q., Chen, X., Wang, G., Qin, Z., Ding, X., 2021. Geological-petrophysical insights in the deep Cambrian dolostone reservoirs in Tarim Basin, China. *AAPG (Am. Assoc. Pet. Geol.) Bull.* 105 (11), 2263–2296.
- Lai, J., Liu, B., Li, H., Pang, X., Liu, S., Bao, M., Wang, G., 2022a. Bedding parallel fractures in fine-grained sedimentary rocks: recognition, formation mechanisms, and prediction using well log. *Petrol. Sci.* 19 (2), 554–569.
- Lai, J., Li, D., Ai, Y., Liu, H., Cai, D., Chen, K., Xie, Y., Wang, G., 2022b. Structural diagenesis in ultra-deep tight sandstones in Kuqa depression, Tarim Basin, China. *Solid Earth* 13, 975–1002.
- Lai, J., Wang, G., Fan, Q., Pang, X., Li, H., Zhao, F., Li, Y., Zhao, X., Zhao, Y., Huang, Y., Bao, M., Qin, Z., Wang, Q., 2022c. Geophysical well log evaluation in the era of unconventional hydrocarbon resources: a review on current status and prospects. *Surv. Geophys.* 43, 913–957.
- Lai, J., Wang, G., Fan, Q., Zhao, F., Zhao, X., Li, Y., Zhao, Y., Pang, X., 2023. Towards the scientific interpretation of geophysical well logs: typical misunderstandings and countermeasures. *Surv. Geophys.* 44, 463–494.
- Lander, R.H., Walderhaug, O., 1999. Porosity prediction through simulation of sandstone compaction and quartz cementation. *AAPG (Am. Assoc. Pet. Geol.) Bull.* 83, 433–449.
- Laubach, S.E., 2003. Practical approaches to identifying sealed and open fractures. *AAPG (Am. Assoc. Pet. Geol.) Bull.* 87 (4), 561–579.
- Laubach, S.E., Eichhubl, P., Hilgers, C., Lander, R.H., 2010. Structural diagenesis. *J. Struct. Geol.* 32 (12), 1866–1872.
- Laubach, S.E., Lander, R.H., Criscenti, L.J., Anovitz, L.M., Urai, J.L., Pollyea, R.M., Hooker, J.N., Narr, W., Evans, M.A., Kerisit, S.N., Olson, J.E., Dewers, T., Fisher, D., Bodnar, R., Evans, B., Dove, P., Bonnell, L.M., Marder, M.P., Pyrak-Nolte, L., 2019. The role of chemistry in fracture pattern development and opportunities to advance interpretations of geological materials. *Rev. Geophys.* 57 (3), 1065–1111.
- Lorenz, J.C., 1999. Stress-sensitive reservoirs. *J. Petrol. Technol.* 51 (1), 61–63.
- Lyu, W., Zeng, L., Zhang, B., Miao, F., Lyu, P., Dong, S., 2017. Influence of natural fractures on gas accumulation in the Upper Triassic tight gas sandstones in the northwestern Sichuan Basin, China. *Mar. Petrol. Geol.* 83, 60–72.
- Lyu, Wenya, Zeng, Lianbo, Peng, Lyu, Tao, Yi, Dong, Shaoqun, Wang, Shengjiao, Xu, Xiang, Chen, Huan, 2022. Insights into the mechanical stratigraphy and vertical fracture patterns in tight oil sandstones: the Upper Triassic Yanchang Formation in the eastern Ordos Basin, China. *J. Petrol. Sci. Eng.* 212, 110247.
- Mansurbeg, H., Morad, S., Salem, A., Marfil, R., El-Ghali, M.A.K., Nystuen, J.P., Caja, M. A., Amorosi, A., Garcia, G., Iglesia, A.L., 2008. Diagenesis and reservoir quality evolution of Paleocene deep-water, marine sandstones, the Shetland-Faroes Basin. *Br. Continent. Shelf: Mar. Petrol. Geol.* 25, 514–543.
- Morad, S., Al-Ramadan, K., Ketzer, J.M., De Ros, L.F., 2010. The impact of diagenesis on the heterogeneity of sandstone reservoirs: a review of the role of depositional facies and sequence stratigraphy. *AAPG (Am. Assoc. Pet. Geol.) Bull.* 94 (8), 1267–1309. <https://doi.org/10.1306/04211009178>.
- Nabawy, B.S., 2018. Impacts of fossil anisotropy on the electric and permeability anisotropy of highly fossiliferous limestone: a case study. *Mar. Geophys. Res.* 39 (4), 537–550.
- Nelson, R.A., 2001. *Geologic Analysis of Naturally Fractured Reservoirs*, second ed. Gulf Professional Publishing, Woburn, Massachusetts, p. 332.
- Nian, T., Wang, G., Xiao, C., Zhou, L., Deng, L., Li, R., 2016. The in situ stress determination from borehole image logs in the Kuqa Depression. *J. Nat. Gas Sci. Eng.* 34, 1077–1084.
- Nian, T., Wang, G., Song, H., 2017. Open tensile fractures at depth in anticlines: a case study in the Tarim basin, NW China. *Terra Nova* 29 (3), 183–190.
- Nian, T., Wang, G., Tan, C., Fei, L., He, W., Wang, S., 2021. Hydraulic apertures of barren fractures in tight-gas sandstones at depth: image-core calibration in the lower cretaceous Bashijiqike Formation, Tarim Basin. *J. Petrol. Sci. Eng.* 196, 108016.
- Nie, X., Zou, C., Pan, L., Huang, Z., Liu, D., 2013. Fracture analysis and determination of in-situ stress direction from resistivity and acoustic image logs and core data in the Wenchuan Earthquake Fault Scientific Drilling Borehole-2 (50–1370 m). *Tectonophysics* 593, 161–171.
- Nygard, R., Gutierrez, M., Gautam, R., Hoeg, K., 2004. Compaction behavior of argillaceous sediments as function of diagenesis. *Mar. Petrol. Geol.* 21, 349–362.
- Ozkan, A., Cumella, S.P., Milliken, K.L., Laubach, S.E., 2011. Prediction of lithofacies and reservoir quality using well logs, late cretaceous Williams Fork formation, Mamm Creek field, Piceance basin, Colorado. *AAPG (Am. Assoc. Pet. Geol.) Bull.* 95 (10), 1699–1723.
- Pang, Xiaojiao, Wang, Guiwen, Kuang, Lichun, Jin, Lai, Gao Yang, Zhao, Yidi, Li, Hongbin, Wang, Song, Bao, Meng, Liu, Shichen, 2022. Prediction of multiscale laminae structure and reservoir quality in fine-grained sedimentary rocks: the Permian Lucaogou Formation in Jimusar Sag, Junggar Basin. *Petrol. Sci.* 19, 2549–2571.
- Paxton, S., Szabo, J., Ajdukiewicz, J., Klimentidis, R., 2002. Construction of an intergranular volume compaction curve for evaluating and predicting compaction

- and porosity loss in rigid-grain sandstone reservoirs. *AAPG (Am. Assoc. Pet. Geol.) Bull.* 86, 2047–2067.
- Poppelreiter, M., Garcia-Carballido, C., Kraaijveld, M., 2010. Borehole image log technology: application across the exploration and production life cycle. In: Poppelreiter, M., Garcia-Carballido, C., Kraaijveld, M. (Eds.), *Dipmeter and Borehole Image Log Technology: AAPG Memoir 92*, pp. 1–13.
- Radwan, A.A., Nabawy, B.S., Abdelmaksoud, A., Lashin, A., 2021. Integrated sedimentological and petrophysical characterization for clastic reservoirs: a case study from New Zealand. *J. Nat. Gas Sci. Eng.* 88, 103797.
- Ramm, M., 2000. Reservoir quality and its relationship to facies and provenance in Middle to Upper Jurassic sequences, northeastern North Sea. *Clay Miner.* 35, 77–94.
- Rossi, C., Marfil, R., Ramseyer, K., Permanyer, A., 2001. Facies-related diagenesis and multiphase siderite cementation and dissolution in the reservoir sandstones of the Khatatba Formation, Egypt's Western Desert. *J. Sediment. Res.* 71, 459–472.
- Salem, A.M., Ketzner, J.M., Morad, S., Rizk, R.R., Al-Aasm, I.S., 2005. Diagenesis and reservoir-quality evolution of incised-valley sandstones: evidence from the Abu Madi gas reservoirs (Upper Miocene), the Nile delta basin, Egypt. *J. Sediment. Res.* 75, 572–584.
- Shen, Y., Lü, X., Guo, S., Song, X., Zhao, J., 2017. Effective evaluation of gas migration in deep and ultra-deep tight sandstone reservoirs of Keshen structural belt, Kuqa depression. *J. Nat. Gas Sci. Eng.* 46, 119–131.
- Shi, G., Zhou, X., Zhang, G., Shi, X., Li, H., 2004. The use of artificial neural network analysis and multiple regression for trap quality evaluation: a case study of the Northern Kuqa Depression of Tarim Basin in western China. *Mar. Petrol. Geol.* 21, 411–420.
- Solano, N., Zambrano, L., Aguilera, R., 2011. Cumulative-gas-production distribution on the Nikanassin formation, Alberta and British Columbia, Canada. *SPE Reservoir Eval. Eng.* 14, 357–376.
- Sun, S., Hou, G., Zheng, C., 2017. Fracture zones constrained by neutral surfaces in a fault-related fold: insights from the Kelasu tectonic zone, Kuqa depression. *J. Struct. Geol.* 104, 112–124.
- Teng, C., Cai, Z., Hao, F., Cao, Z., 2020. Structural geometry and evolution of an intracratonic strike-slip fault zone: a case study from the north SB5 fault zone in the Tarim Basin, China. *J. Struct. Geol.* 140, 104159.
- Tobin, R.C., McClain, T., Lieber, R.B., Ozkan, A., Banfield, L.A., Marchand, A.M.E., McRae, L.E., 2010. Reservoir quality modeling of tight-gas sands in Wamsutter field: integration of diagenesis, petroleum systems, and production data. *AAPG (Am. Assoc. Pet. Geol.) Bull.* 94 (8), 1229–1266.
- Wang, J., Wang, H., Chen, H., Jiang, S., Zhao, S., 2013. Responses of two lithosomes of Lower Cretaceous coarse clastic rocks to tectonism in Kuqa foreland sub-basin, Northern Tarim Basin, Northwest China. *Sediment. Geol.* 289, 182–193.
- Weber, J., Ricken, W., 2005. Quartz cementation and related sedimentary architecture of the Triassic solling formation, Reinhardswald basin, Germany. *Sediment. Geol.* 175, 459–477.
- Wu, D., Liu, S., Chen, H., Lin, L., Yu, Y., Xu, C., Pan, B., 2020. Investigation and prediction of diagenetic facies using well logs in tight gas reservoirs: evidences from the Xu-2 member in the Xinchang structural belt of the western Sichuan Basin, western China. *J. Petrol. Sci. Eng.* 192, 107326.
- Xin, Yi, Wang, Guiwen, Liu, Bingchang, Ai, Yong, Cai, Deyang, Yang, Shuwen, Liu, Hongkun, Xie, Yuqiang, Chen, Kangjun, 2022. Pore structure evaluation in ultra-deep tight sandstones using NMR measurements and fractal analysis. *J. Petrol. Sci. Eng.* 211, 110180.
- Xu, S., Lu, X., Sun, Z., Pi, X., Liu, L., Li, Q., Xie, H., 2004. Kela-2: a major gas field in the Tarim Basin of west China. *Petrol. Geosci.* 10, 95–106.
- Zeng, L., 2010. Microfracturing in the upper Triassic Sichuan basin tight-gas sandstones: tectonic, overpressure, and diagenetic origins. *AAPG (Am. Assoc. Pet. Geol.) Bull.* 94 (12), 1811–1825.
- Zeng, L.B., Wang, H.J., Gong, L., Liu, B.M., 2010. Impacts of the tectonic stress field on natural gas migration and accumulation: a case study of the Kuqa Depression in the Tarim Basin, China. *Mar. Petrol. Geol.* 27, 1616–1627.
- Zhang, S.C., Huang, H.P., 2005. Geochemistry of Palaeozoic marine petroleum from the Tarim Basin, NW China: Part 1. Oil family classification. *Org. Geochem.* 36, 1204–1214.
- Zhang, Y., Pe-Piper, G., Piper, D.J.W., 2015. How sandstone porosity and permeability vary with diagenetic minerals in the Scotian Basin, offshore Eastern Canada: implications for reservoir quality. *Mar. Petrol. Geol.* 63, 28–45.
- Zhang, Q., Wu, Xin-Song, Radwan, A.E., Wang, B., Wang, K., Tian, H., Yin, S., 2022. Diagenesis of continental tight sandstone and its control on reservoir quality: a case study of the Quan 3 member of the cretaceous Quantou Formation, Fuxin uplift, Songliao Basin. *Mar. Petrol. Geol.* 145, 105883.
- Zheng, C., Sun, X., Hou, G., 2020. Discrete-element numerical modeling of sub-salt structures in the Central Kelasu fold-thrust belt, Kuqa Depression, northwestern China. *J. Geodyn.* 134, 101687.
- Zhong, G.F., Ma, Z.T., Liu, R.L., Wu, N.F., 2003. Distribution of upper Cenozoic carbonate-cemented sandstones, Kuche depression, northwest China: insights from high-resolution borehole micro-resistivity imaging. *J. Sediment. Res.* 73 (2), 177–186.
- Zou, Y., Zhao, C., Wang, Y., Zhao, W., Peng, P., Shuai, Y., 2006. Characteristics and origin of natural gases in the Kuqa depression of Tarim basin, NW China. *Org. Geochem.* 37, 280–290.
- Zou, C.N., Zhu, R.K., Liu, K.Y., Su, L., Bai, B., Zhang, X.X., Yuan, X.J., Wang, J.H., 2012. Tight gas sandstone reservoirs in China: characteristics and recognition criteria. *J. Petrol. Sci. Eng.* 88–89, 82–91.